

## RESEARCH ARTICLE

# miR-322 stabilizes MEK1 expression to inhibit RAF/MEK/ERK pathway activation in cartilage

Björn Bluhm<sup>1,2</sup>, Harald W. A. Ehlen<sup>1,2</sup>, Tatjana Holzer<sup>1,2</sup>, Veronika S. Georgieva<sup>1,2</sup>, Juliane Heilig<sup>3,4</sup>, Lena Pitzler<sup>1,2</sup>, Julia Etich<sup>1,2</sup>, Toman Bortecen<sup>1,2</sup>, Christian Frie<sup>1,2</sup>, Kristina Probst<sup>1,2</sup>, Anja Niehoff<sup>3,4</sup>, Daniele Belluoccio<sup>5,6</sup>, Jocelyn Van den Bergen<sup>5,7</sup> and Bent Brachvogel<sup>1,2,4,\*</sup>

**ABSTRACT**

Cartilage originates from mesenchymal cell condensations that differentiate into chondrocytes of transient growth plate cartilage or permanent cartilage of the articular joint surface and trachea. MicroRNAs fine-tune the activation of entire signaling networks and thereby modulate complex cellular responses, but so far only limited data are available on miRNAs that regulate cartilage development. Here, we characterize a miRNA that promotes the biosynthesis of a key component in the RAF/MEK/ERK pathway in cartilage. Specifically, by transcriptome profiling we identified miR-322 to be upregulated during chondrocyte differentiation. Among the various miR-322 target genes in the RAF/MEK/ERK pathway, only *Mek1* was identified as a regulated target in chondrocytes. Surprisingly, an increased concentration of miR-322 stabilizes *Mek1* mRNA to raise protein levels and dampen ERK1/2 phosphorylation, while cartilage-specific inactivation of miR322 in mice linked the loss of miR-322 to decreased MEK1 levels and to increased RAF/MEK/ERK pathway activation. Such mice died perinatally due to tracheal growth restriction and respiratory failure. Hence, a single miRNA can stimulate the production of an inhibitory component of a central signaling pathway to impair cartilage development.

**KEY WORDS:** MEK, Cartilage, MAPK, miR-322, CRISPR, Stabilization

**INTRODUCTION**

Cartilage is composed of chondrocytes, a cell type derived from condensations of mesenchymal precursor cells. During development, chondrocytes in the cartilage anlagen become arranged into parallel stacks to form the temporary cartilage growth plates (Wuelling and Vortkamp, 2011), whereas interzonal mesenchymal cells between neighboring cartilage anlagen differentiate into permanent joint articular cartilage (Decker et al., 2017). Likewise, precartilaginous mesenchymal nodules surrounding the trachea differentiate into chondrocytes of the permanent tracheal cartilage (Sher and Liu,

2016). Each cartilaginous tissue has a specific function in the musculoskeletal system. The growth plate cartilage intermediate directs longitudinal growth of most parts of the skeleton and is later transformed into bone tissue, whereas the permanent joint articular cartilage provides a smooth and stable joint surface to preserve mobility throughout life. The tracheal cartilage is needed to build flexible but stiff rings that resist breathing forces to maintain the air flow into the lungs.


To fulfil the diverse functions according to their location, chondrocytes have to interpret their microenvironment. The RAF/MEK/ERK pathway is used by many cells to translate extracellular signals into intracellular responses and adapt their cell phenotype. Growth factor signals can activate the rapidly accelerated fibrosarcoma (RAF) kinase to stimulate the mitogen-activated protein kinase (MEK1/2) and the extracellular signal-regulated kinases 1 and 2 (ERK1/2) to induce specific differentiation and activation programs in cells. Changes in RAF/MEK/ERK pathway activation are linked to a number of human skeletal syndromes and cartilage-specific inactivation of pathway components in mice can cause chondrodysplasia, bone growth alterations (Matsushita and Murakami, 2012) and fatal tracheal cartilage disorganization (Boucherat et al., 2014). Hence, the pathway is of general importance for cartilage homeostasis.

The activation of the RAF/MEK/ERK kinase cascade is tightly controlled at various levels. Formation of homo-/heterodimers, organization in scaffolds and differential phosphorylation contribute to the regulation of the pathway. In addition, changes in levels of individual kinases can alter the strength and duration of pathway activation (Catalanotti et al., 2009) and post-transcriptional regulation by microRNAs (miRNA) may add another layer of complexity. These small RNA molecules can bind to complementary sequences of mRNA targets to inhibit their expression and modulate the activation of entire signaling pathways. First evidence for a crucial role for miRNAs in cartilage was found through the reduction of global miRNA amounts using Col2a1-Cre-mediated deletion of the miRNA processing enzyme Dicer in mice (Gradus et al., 2011; Kobayashi et al., 2008). This led to skeletal defects and the transgenic mice died shortly after birth due to a collapse of the cartilaginous trachea (Gradus et al., 2011). The phenotype partly resembled the situation in mice with a genetically inactivated RAF/MEK/ERK pathway in cartilaginous tissues (Boucherat et al., 2014), but the contribution of a specific miRNA has not been defined.

We have recently characterized a miRNA that can modulate matrix-dependent cell migration and intercellular interaction (Pitzler et al., 2016), developed approaches to characterize cartilage differentiation *in situ* (Belluoccio et al., 2010a) and successfully applied the methods to characterize a novel miRNA (miR-26a) that

<sup>1</sup>Department of Pediatrics and Adolescent Medicine, Experimental Neonatology, Medical Faculty, University of Cologne, Cologne 50931, Germany. <sup>2</sup>Center for Biochemistry, Medical Faculty, University of Cologne, Cologne 50931, Germany. <sup>3</sup>Institute of Biomechanics and Orthopaedics, German Sport University Cologne, Cologne 50931, Germany. <sup>4</sup>Cologne Center for Musculoskeletal Biomechanics (CCMB), University of Cologne, Cologne 50931, Germany. <sup>5</sup>Murdoch Children's Research Institute, University of Melbourne, Parkville, Victoria 3052, Australia. <sup>6</sup>Department of Biochemistry and Molecular Biology, University of Melbourne, Parkville, Victoria 3052, Australia. <sup>7</sup>Department of Pediatrics, University of Melbourne, Parkville, Victoria 3052, Australia.

\*Author for correspondence (bent.brachvogel@uni-koeln.de)

 B.B., 0000-0002-3923-0554; L.P., 0000-0002-6583-8192

modulates ECM homeostasis in chondrocytes (Etich et al., 2015). Here, we used this expertise to identify several known and novel miRNAs that are differentially expressed in growth plate cartilage. Among those, miR-322 was the most abundant highly up-regulated miRNA of the prehypertrophic and hypertrophic growth plate cartilage. According to bioinformatic analysis, the RAF/MEK/ERK signaling pathway was one of the highest ranked pathways regulated by miR-322. A detailed analysis of RAF/MEK/ERK pathway regulation showed that miR-322 promotes MEK1 production to suppress ERK1/2 phosphorylation and pathway activation in chondrocytes. Loss of miR-322 signal in cartilage of transgenic mice manifests in a decrease of the hypertrophic growth plate, in a reduction of the diameter of tracheal cartilage rings and the impairment of tracheal lumen organization with fatal consequences for survival. Collectively, these findings demonstrate that miR-322 is an unconventional inhibitor of a central signaling pathway in chondrocytes that regulates transient and permanent cartilage homeostasis.

## RESULTS

### miR-322 is differentially expressed during cartilage development

To characterize miRNAs that are regulated during cartilage differentiation, microdissected material from the femoral growth plates of 12-day-old mice was subjected to microarray analysis. Among the 690 analyzed miRNAs of the miRBaseV14 (Fig. 1A), several were significantly upregulated in prehypertrophic and hypertrophic zones of the growth plate cartilage. Four miRNAs were strongly increased, namely miR-181a, miR-181a\*, miR-322 and miR-503 (Fig. 1B). The expression profile was then studied by qPCR analysis (Fig. 1C,D). A strong upregulation in the prehypertrophic/hypertrophic zone could be confirmed for miR-181a, miR-181a\* and miR-322, whereas miR-140 and the antisense strands miR-140\* and miR-322\* were not differentially expressed. Non-specific products were amplified for miR-503 in qPCR and its upregulation could therefore not be validated. Among the upregulated miRNAs, only miR-181a and miR-181a\* have previously been described to be differentially expressed during chondrogenesis and to be among the most interesting candidates to be studied in endochondral ossification (Gabler et al., 2015). However, loss of miR-181a in transgenic mice was not associated with an obvious skeletal phenotype (Henaoui-Mejia et al., 2013). Therefore, we focused the analysis on the newly identified miR-322, which showed the strongest intensity expression values of all upregulated miRNAs *in situ*. For this miRNA, we could also demonstrate an upregulation upon differentiation of ATDC5 cells into prehypertrophic/hypertrophic chondrocyte-like cells using high density cultures (Fig. 1E). Chondrogenic differentiation was demonstrated by Alcian Blue staining for proteoglycan deposition (Fig. 1F) as well as by *Col2a1*, *Acan* and miR-140 expression (Fig. 1G,F), prehypertrophic/hypertrophic differentiation by *Pth1r*, *Cd200*, *Col10a1* and *Mmp13* expression (Fig. 1G).

### miR-322 inhibits RAF/MEK/ERK pathway activation in chondrocytes

To obtain insights into the potential molecular function of miR-322 in chondrocytes, we performed a string database search of the 1947 predicted target genes (TargetsCan 6.1) expressed in growth plate cartilage. Genes associated with intracellular components, as well as with the PI3K-AKT and insulin signaling pathways, were among the highest ranked targets of the miR-322 according to Gene Ontology cellular component and KEGG analysis (Fig. S1).

Therefore, the activation of both pathways was studied after increasing miR-322 levels in primary epiphyseal chondrocytes (PECs). Cells were transfected with control or miR-322 mimic oligonucleotides, stimulated with insulin and phosphorylation of AKT, and ERK1/2 levels were determined by immunoblot analysis (Fig. 2A). Phosphorylation of AKT was induced by insulin, but was the same in control- and miR-322 mimic-transfected cells. By contrast, ERK1/2 phosphorylation was significantly decreased in miR-322 mimic-transfected PECs 5 and 10 min after stimulation when compared with control. The total amounts of AKT and ERK1/2 were not altered between control- and miR-322 mimic-transfected PECs. These results show that miR-322 specifically inhibits the phosphorylation of ERK1/2 in PECs.

### miR-322 significantly increases MEK1/2 levels in chondrocytes

Several target genes of the miR-322 upstream of ERK1/2 were predicted for the RAF/MEK/ERK pathway and we next studied the interaction of miR-322 with the core binding sequence of the target genes using luciferase assays (Fig. 2B). HEK293 cells were used due to insufficient transfection of the luciferase vector and low expression of the luciferase reporter in PECs. The luciferase activity was strongly decreased in miR-322 mimic-transfected HEK293 cells that contained the binding sequence of *Igf1r*, *Raf* and *Mek1* in the 3'-UTR of the luciferase reporter gene, but not in cells that contained a binding sequence of *Insr*, *Igf2r* or *Erk1*. Two mutations within the binding sequence of *Igf1r*, *Raf1* and *Mek1* (Fig. S2) eliminated the inhibitory effect of miR-322, pointing to a specific interaction between miR-322 and the 3'-UTR of those mRNAs. Next, we determined the expression of targeted genes linked to the activation of the RAF/MEK/ERK pathway in control- and miR-322 mimic-transfected PECs by immunoblot analysis (Fig. 2C). Similar amounts of IGF1R, INSR, PRKCI, RAC1/2/3 and c-RAF were detected 2 and 3 days after transfection. Surprisingly, MEK1/2 levels were significantly increased, whereas ERK1/2 levels were not altered when using pan-specific antibodies. miRNAs normally inhibit the expression of genes and only few miRNAs have been described to stabilize mRNAs and stimulate protein expression (Valinezhad Orang et al., 2014), and to our knowledge none of these miRNAs targets an essential component of a signaling pathway needed for cell survival, proliferation and differentiation. Hence, we focused the analysis on MEK1/2 expression changes in miR-322 mimic-transfected cells.

### miR-322 stabilizes *Mek1* mRNA to raise MEK1 protein levels

In miR-322 mimic-transfected chondrocytes, only MEK1 protein levels were increased, as shown by immunoblot analysis using MEK1/2-pan, MEK1- and MEK2-specific antibodies (Fig. 3A). Transfection of a *Mek1*-specific siRNA could normalize MEK1 protein levels in miR-322 mimic-transfected chondrocytes, whereas MEK2 protein abundance was not changed. Presumably, miR-322 prevents degradation of the mRNA to increase the biosynthesis of MEK1 protein and therefore the relative mRNA levels were analyzed by qPCR analysis (Fig. 3B). A significant 1.6-fold increase in *Mek1* mRNA was detected in miR-322 mimic-transfected chondrocytes compared with control-transfected PECs, whereas mRNA levels of the predicted targets *Raf1* and *Erk1* were not significantly altered. We also blocked gene transcription with actinomycin D in the transfected PECs and followed the kinetics of mRNA degradation by qPCR analysis. The degradation of the *Mek1* mRNA was significantly delayed by ~8 h

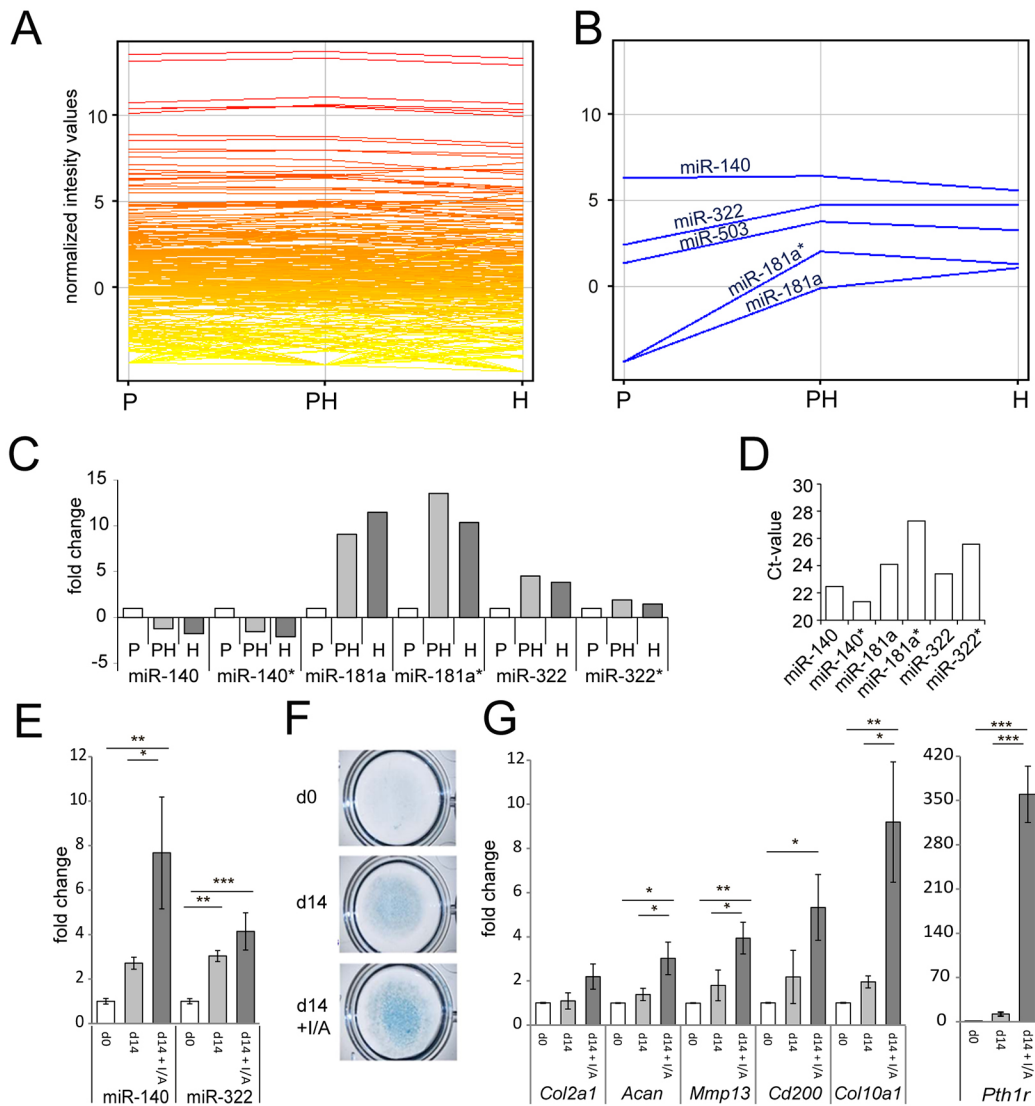


**Fig. 1. Identification of miRNAs regulated during endochondral ossification within the mouse growth plate.** The miRNA transcriptome was compared between the proliferative, prehypertrophic and hypertrophic zones of growth plate cartilage of femora from 12-day-old mice using miRNA array (Agilent) analyses based on the Sanger miRBase release 14. (A) Intensity plot includes all miRNAs detected in chondrocytes. P, proliferative zone; PH, prehypertrophic zone; H, hypertrophic zone. (B) Plot of miRNAs differentially expressed in prehypertrophic/hypertrophic chondrocytes (fold-change  $\geq 4$ ,  $P \geq 0.005$ , P versus PH). Microarray analyses were performed in two independent biological experiments. Log<sub>2</sub>-transformed intensity values are shown. (C) The relative expression changes of selected miRNAs were confirmed by qPCR using material from two independent RNA isolations. (D) The Ct-values are given. (E) ATDC5 cells were cultured at high density in the absence and presence of insulin-transferrin-selenium and ascorbate (+I/A) to induce chondrogenic differentiation. The relative expression of (E) miR-140 and miR-322, as well as of the chondrocyte-specific genes (G) *Col2a1* and *Acan* and the prehypertrophic/hypertrophic zone-specific genes *Mmp13*, *Cd200*, *Col10a1* and *Pth1r* were determined by qPCR.  $\beta$ -Actin and miR-92 expression were used for normalization. The standard deviations ( $n=3$ ) and significances are shown. (F) Cultures were stained with Alcian Blue to detect proteoglycan deposition.

in miR-322 mimic-transfected PECs compared with control (Fig. 3C, Fig. S3A).

To determine whether the miR-322-mediated increase in *Mek1* expression was independent of RAF/MEK/ERK pathway stimulation, we cultured control- and miR-322 mimic-transfected chondrocytes in the presence of the pathway inhibitor U0126 (Pitzler et al., 2016) and determined pERK/ERK and MEK1 levels by immunoblot analysis. Phosphorylation of ERK was induced by insulin in control- and miR-322 mimic-transfected chondrocytes, but not in the presence of the inhibitor (Fig. 3D). MEK1 levels were increased in miR-322 mimic-transfected chondrocytes in the absence or presence of U0126 compared with control (Fig. 3D). The results indicate that miR-322 interacts directly with *Mek1* mRNA irrespective of RAF/MEK/ERK pathway activation.

#### CRISPR/Cas-mediated genomic deletion of the miR-322-specific binding site in *Mek1* reduces MEK1 protein levels in miR-322 mimic-transfected cells

To provide genetic evidence for this interaction and to rule out indirect effects of miR-322 on *Mek1* expression, we finally used CRISPR/Cas-mediated genomic engineering (Sander and Joung, 2014) in chondrogenic ATDC5 cells to delete the miR-322-specific binding site ( $\pm 50$  bp) in the 3'-UTR of *Mek1* (Fig. S3B,D). PCR-based genotyping of 48 generated cell clones showed that 32 clones had the miR-322-specific binding site on both alleles (+/+), whereas 15 clones had a monoallelic (+/-) and one clone a biallelic (-/-) deletion of the binding sequence (Fig. 3E). The homozygous clone with the biallelic deletion and a single wild-type clone were expanded, transfected with control or miR-322 mimic

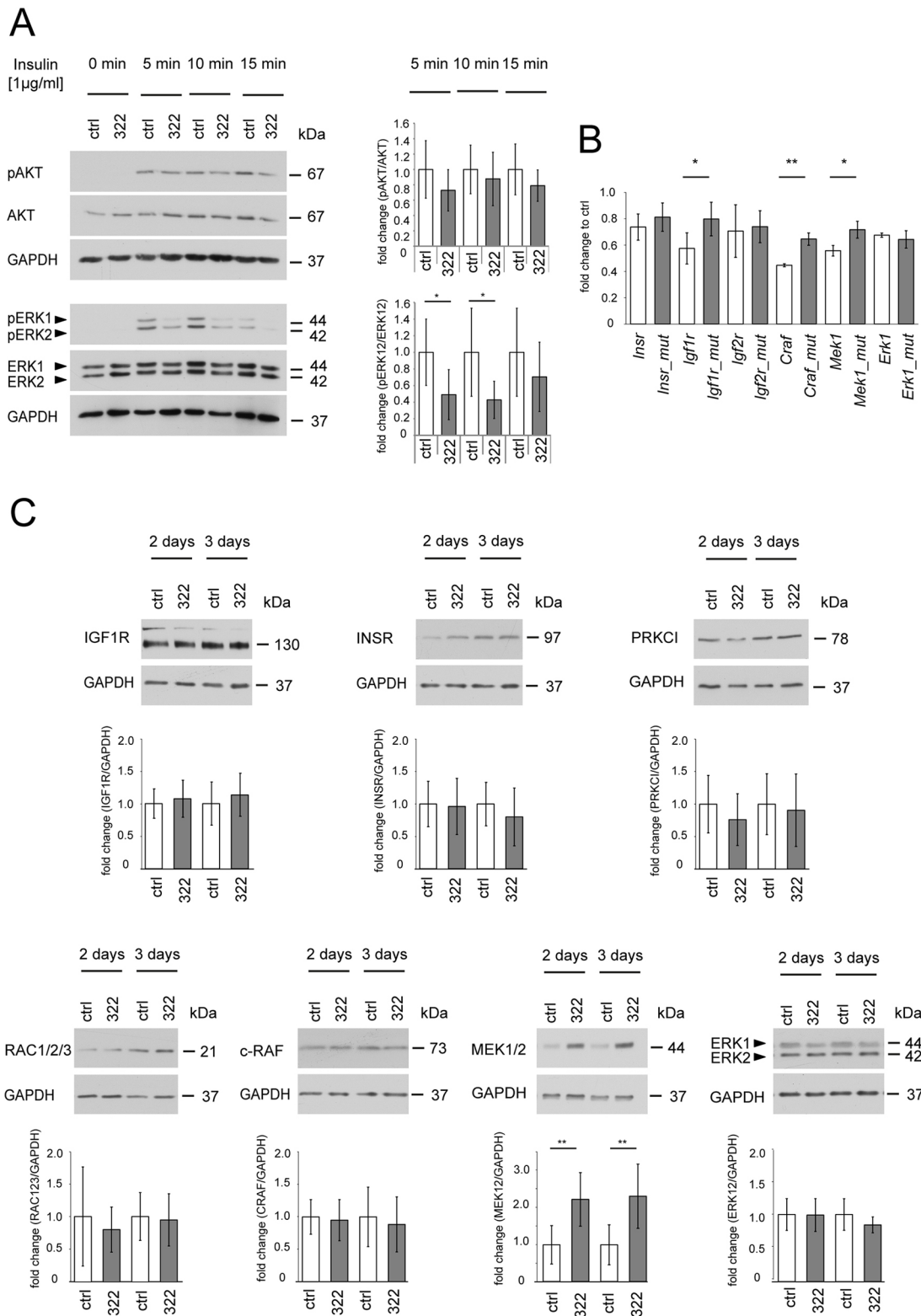


**Fig. 2. Activation of miR-322-dependent signaling pathways and identification of targets.** Analysis of AKT and ERK1/2 signaling pathway activation after insulin stimulation in (A) miR-322 mimic-transfected (322) primary epiphyseal chondrocytes (PECs) compared with control-transfected (ctrl) PECs. Representative immunoblots show phosphorylated AKT (pAKT), total AKT (upper panel), phosphorylated ERK1/2 (pERK1/2), total ERK1/2 (lower panel) and GAPDH. The fold-change in phosphorylation in miR-322 mimic-transfected PECs compared with control-transfected PECs normalized to total AKT or ERK1/2 was determined. The results of four independent experiments are summarized (graphs). (B) Interaction of miR-322 with the intact or mutated (mut) putative binding site in the 3'-UTR of the indicated target mRNAs. Fold-changes of Renilla to Firefly luciferase activity in miR-322 mimic-transfected HEK cells compared with control are presented ( $\geq 3$ ). (C) Extracts of control- and miR-322 mimic-transfected PECs analyzed for the presence of IGF1R, INSR, PRKCI, RAC1/2/3, c-RAF, MEK1/2 and ERK1/2 by immunoblot analysis. GAPDH detection was used as loading control. Fold-change of targets to GAPDH ratio in miR-322 mimic-transfected PECs compared with control is shown as the analysis of three independent experiments (graphs).

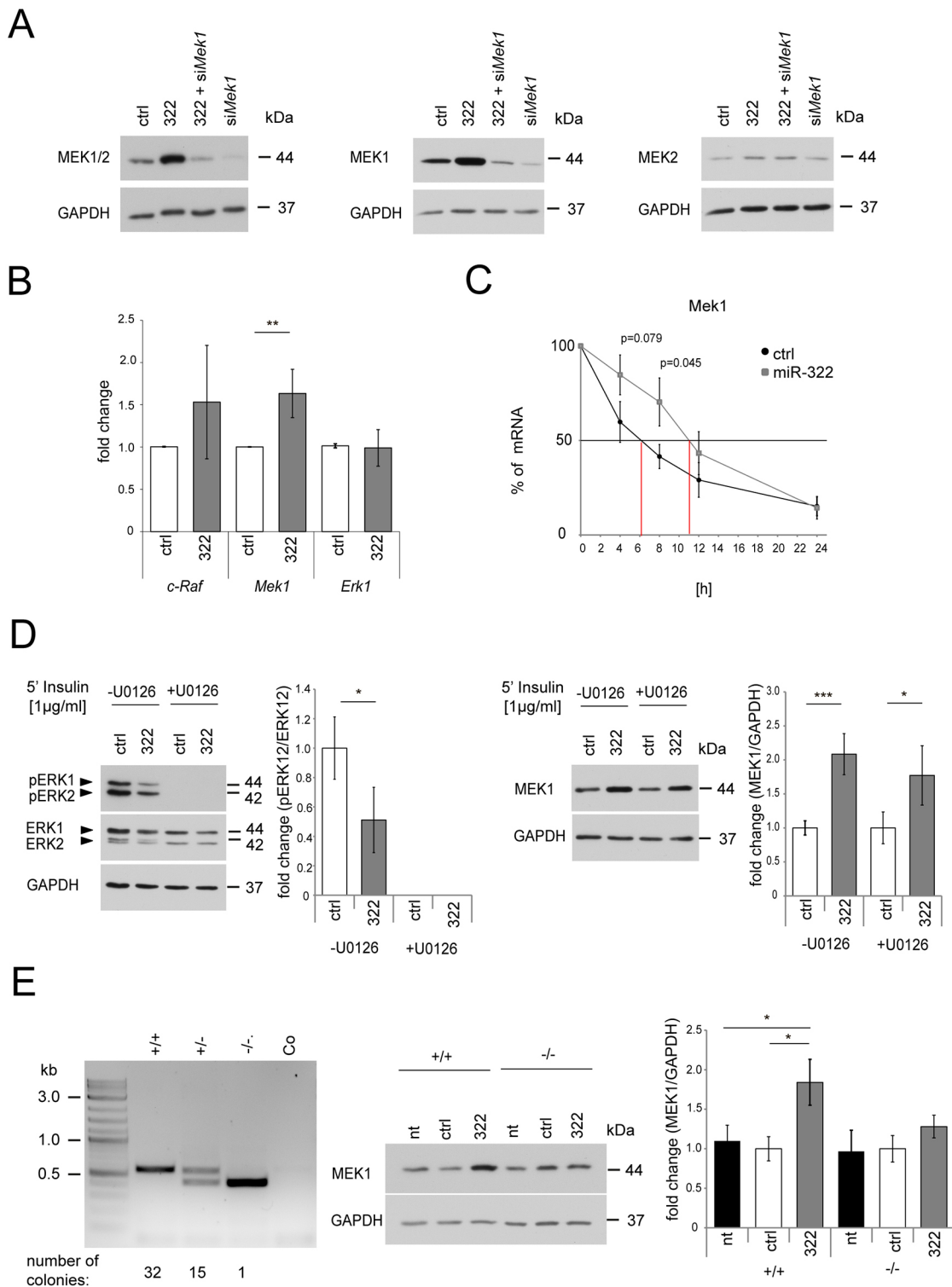


**Fig. 3. MEK1/2 regulation in control- or miR-322 mimic-transfected PECs.** (A) Immunoblot analysis of total MEK1/2 (left), MEK1 (center) and MEK2 (right) protein levels in control- (ctrl), miR-322 (322) mimic-, miR-322 mimic/*Mek1*-siRNA (322+*siMek1*)- or *Mek1*-siRNA- (*siMek1*) transfected PECs. (B) *Raf1*, *Mek1* and *Erk1* expression in miR-322 mimic-transfected PECs was compared with control transfected cells using qPCR analysis. The evaluation of six independent biological experiments is shown. (C) *Mek1* mRNA decay in control- and miR-322 mimic-transfected PECs was determined by qPCR analysis at various time points after blocking gene transcription with actinomycin D. The summary of three independent experiments is given (graph). Data are mean $\pm$ s.d. and  $t_{1/2}$  values are marked. (D) Characterization of ERK1/2 signaling pathway activation (left) and MEK1 stabilization (right) after insulin stimulation in miR-322 mimic-transfected PECs and control-transfected PECs in the presence and absence of 10  $\mu$ M U0126. Fold-changes of ERK1/2 phosphorylation and MEK1 levels for four independent experiments are shown (graphs). (E) PCR and immunoblot analysis of CRISPR/Cas engineered ATDC5 cells. The corresponding PCR products for wild-type (+/+), heterozygous (+/-) or biallelic (-/-) deletions of the miR-322-specific binding site in the 3'UTR of *Mek1* are shown (left). The negative control (Co) contains no genomic DNA. (Center) Immunoblot analysis of total MEK1 and GAPDH levels in control- and miR-322 mimic-transfected ATDC5 cells containing the wild-type (+/+) or biallelic deletion (-/-) of the miR-322 binding site in the 3'-UTR of *Mek1*. Quantification of MEK1 levels is shown (graph).

oligonucleotides, and the MEK1 levels were determined by immunoblot analysis. MEK1 levels were significantly increased in miR-322 mimic-transfected ATDC5 cells containing the wild-type binding site when compared with control- or non-transfected cells (Fig. 3E, center, Fig. S3). In contrast, MEK1 levels were not increased in miR-322 mimic-transfected ATDC5 cells with a biallelic deletion of the miR-322-specific interaction sites in the 3'-UTR of *Mek1*. Hence, the miR-322-specific binding site is essential to stabilize *Mek1* mRNA, increase MEK1 protein levels, and presumably inhibit ERK1/2 phosphorylation and RAF/MEK/ERK pathway activation in chondrogenic cells.

#### siRNA-mediated silencing of *Mek1* mRNA reverses miR-322 mediated RAF/MEK/ERK pathway inhibition

To demonstrate this link between increased MEK1 levels and pathway activation, we reduced MEK1 protein levels in miR-322 mimic-transfected chondrocytes using *Mek1*-specific siRNA and studied the intensity and duration of ERK1/2 phosphorylation by immunoblot analysis. MEK1/2 protein levels were successfully decreased and ERK1/2 phosphorylation levels were increased in miR-322 mimic/*Mek1*-siRNA co-transfected PECs (Fig. 4A, Fig. S4A,B). The kinetics of ERK1/2 phosphorylation partially resembled those in control-transfected PECs, whereas in miR-322 mimic transfected PECs ERK1/2 phosphorylation was significantly inhibited. Quantification of ERK1/2 phosphorylation (Fig. 4B) confirmed the partial restoration of the pERK1/2 phosphorylation signal after insulin stimulation in miR-322 mimic/*Mek1*-specific siRNA transfected PECs. Changes in cell morphology may also

impact MEK1 levels in miR-322 mimic transfected PECs but we could not observe morphological alteration (Fig. S4C). Hence, the results indicate that miR-322 induced changes in RAF/MEK/ERK pathway activation could be partially reversed by targeting *Mek1* mRNA and that the increase in MEK1 protein levels is the causative link to RAF/MEK/ERK pathway inhibition by miR-322 in chondrocytes.

#### Cartilage-specific deletion of miR-322 results in neonatal death of hemizygous mutants

To analyze the role of miR-322-mediated stabilization of *Mek1* in cartilage development, we studied transgenic mice (Col2a1-*Mirc24<sup>tm1M</sup>*) lacking the expression of miR-322 in cartilaginous tissue. To confirm the cartilage-specific expression, we initially determined the perinatal expression of the X-chromosomal encoded miR-322 cluster in various tissues by detecting *lacZ* reporter gene expression using X-Gal staining (Fig. 5A). The blue product was mainly seen in cartilaginous tissues of the trachea, rib cage and hindlimb, in skeletal muscle and heart, as well as in lung, showing that the cluster is predominately expressed in musculoskeletal tissues. Within the growth plate, staining was found in prehypertrophic/hypertrophic chondrocytes and more distal chondrocytes, but not in proliferative chondrocytes of hemizygous *Mirc24<sup>tm1MY</sup>* males (Fig. 5B). Interestingly, a mosaic-like expression was seen in the growth plate of heterozygous *Mirc24<sup>tm1MX</sup>* females. This demonstrates that miR-322 is specifically expressed in the prehypertrophic/hypertrophic cartilage, and shows that *Mirc24* cluster expression is stochastically silenced on the inactivated

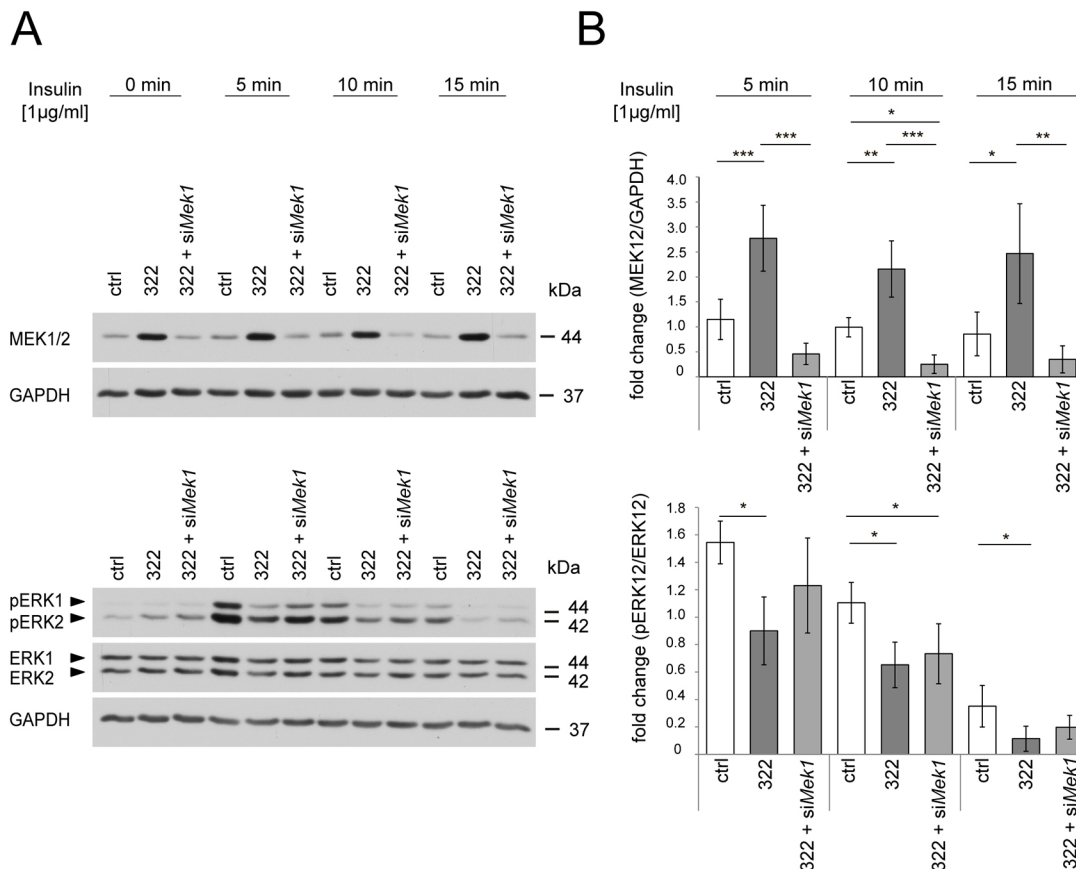


**Fig. 4.** *siMek1*-mediated partial reversion of the RAF/MEK/ERK pathway inhibition in miR-322 mimic-transfected PECs. (A) Representative immunoblots showing total MEK1/2 (upper panel), pERK1/2, total ERK1/2 (lower panel) and GAPDH in control- (ctrl), miR-322 (322) mimic- and miR-322 mimic/*Mek1*-siRNA (322+*siMek1*)-transfected PECs. (B) Quantification of the experiments ( $n \geq 3$ ) is shown (graphs).

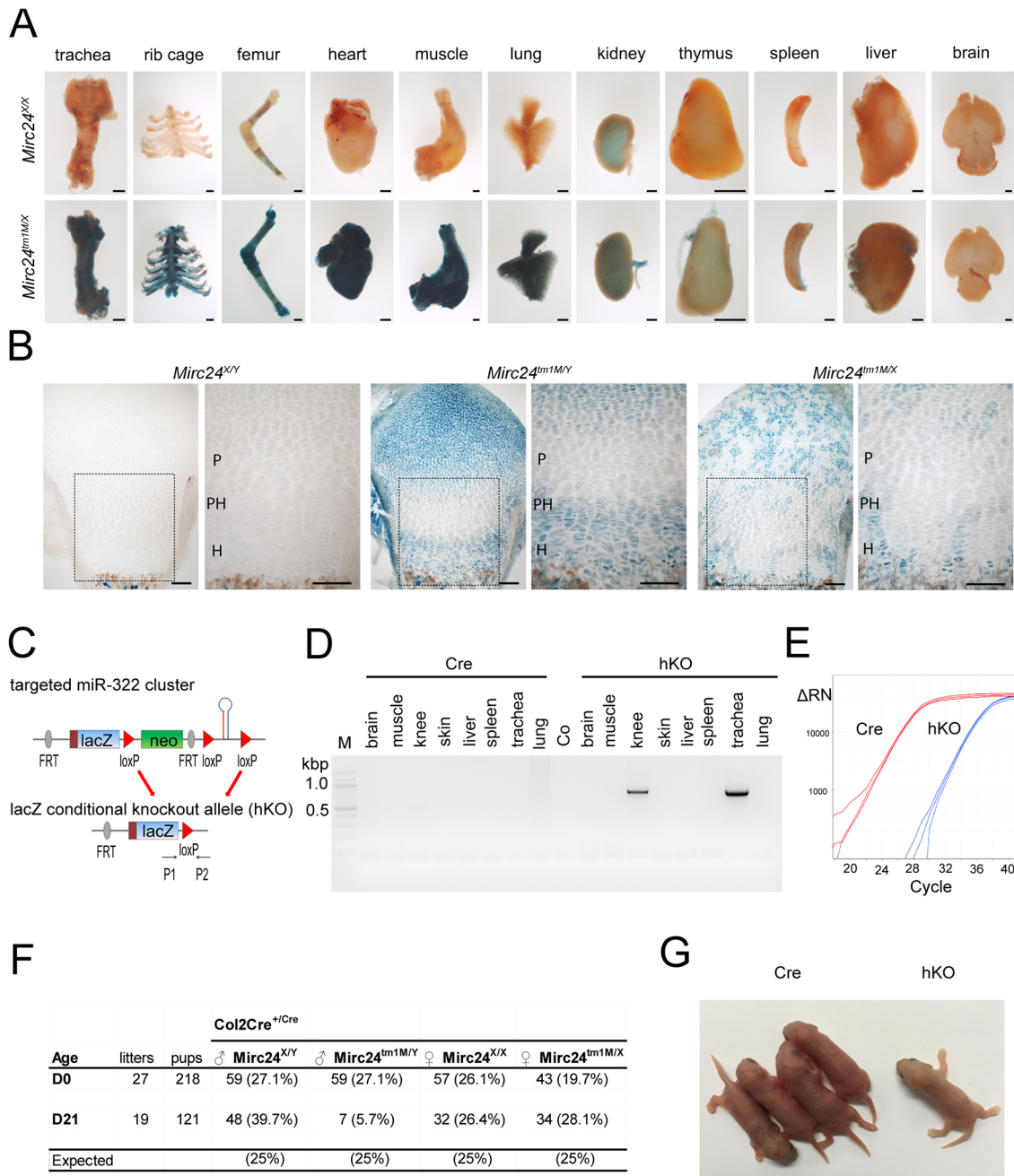


**Fig. 5. Expression and genetic inactivation of the miR-322 cluster in mice.** Expression of the *lacZ* reporter gene in (A) isolated tissues of *Mirc24<sup>xy</sup>* and *Mirc24<sup>tm1Mx</sup>* female newborns and (B) sections of the femoral growth plate of *Mirc24<sup>xy</sup>*, *Mirc24<sup>tm1MY</sup>* male and *Mirc24<sup>tm1Mx</sup>* female newborns was detected by X-Gal staining and assessed by microscopy. The boxed areas in B are enlarged on the right. (C) The *Col2a1*-Cre mediated deletion of the miR-322 cluster located on the X-chromosome in *Col2a1*-Cre-*Mirc24<sup>tm1M</sup>* mice. The organization of the targeted allele prior and after Cre-mediated recombination is shown. The localization of the miR-322 cluster (hairpin), recombination sites (loxP, FRT), the expression (*lacZ*) and resistance cassette (*neo*) are indicated. The binding sites of the primers used for deletion PCR (results in D) are shown (P1, P2). (D) PCR analysis of cartilage-specific cluster deletion in isolated tissues of *Col2a1*-Cre (Cre) and hemizygous *Col2a1*-Cre-*Mirc24<sup>tm1MY</sup>* (hKO) males. (E) The relative expression change of miR-322 in isolated chondrocytes was determined by qPCR analysis. (F) Mendelian inheritance pattern in live offspring of *Col2a1*-Cre×*Mirc24<sup>tm1Mx</sup>* females intercrosses directly after birth (D0) and after 21 days (D21). (G) Overview of Cre and hKO neonatal males. Scale bars: 500 μm in A; 100 μm in B.

X-chromosome in female mice. Floxed *Mirc24<sup>tm1Mx</sup>* female mice were then crossed with males expressing *Col2a1* promoter-driven Cre recombinase (*Col2a1*-Cre) (Ovchinnikov et al., 2000) to produce hemizygous males with a cartilage-specific deletion of *Mirc24* on the X-chromosome (*Col2a1*-Cre-*Mirc24<sup>tm1M</sup>*, Fig. 5C). The specificity and efficiency of deletion was confirmed by genomic PCR and qPCR analysis (Fig. 5D,E), and the Mendelian

inheritance of the deleted allele was determined by PCR in 21-day-old offspring. Only 5.7% hemizygous *Col2a1*-Cre-*Mirc24<sup>tm1M</sup>* males were detected among 121 live offspring, while the percentage of *Col2a1*-Cre (39.7%) male littermates was increased (Fig. 5F). No alterations in the Mendelian inheritance pattern were seen for *Col2a1*-Cre (26.4%) and *Col2a1*-Cre-*Mirc24<sup>tm1M</sup>* (28.1%) females. The results indicate that loss of the miR-322 cluster in

hemizygous *Col2a1-Cre-Mirc24<sup>tm1M</sup>* males affects the survival rate so we then focused on early postnatal development. At birth, 27.1% of *Col2a1-Cre* and 27.1% of *Col2a1-Cre-Mirc24<sup>tm1M</sup>* male littermates, and 26.1% of *Col2a1-Cre* and 19.7% of *Col2a1-Cre-Mirc24<sup>tm1M</sup>* female littermates were found among 218 live offspring. Most of the hemizygous *Col2a1-Cre-Mirc24<sup>tm1M</sup>* males died shortly after birth. These mutants showed no significant weight differences [*Cre* 1.43 g $\pm$ 0.17 (s.d.); *Col2a1-Cre-Mirc24<sup>tm1M/Y</sup>*

(hKO) 1.34 g $\pm$ 0.18], but a pale skin that points to respiratory dysfunction at birth (Fig. 5G).

**Skeletal bone formation is altered in mutants**

The deletion of miR-322 may result in rib cage alterations to impair respiratory function and we therefore assessed bone and cartilage organization in newborn males using Alcian Blue/Alizarin Red S staining for a minimum of six mice per genotype (Fig. 6A). The

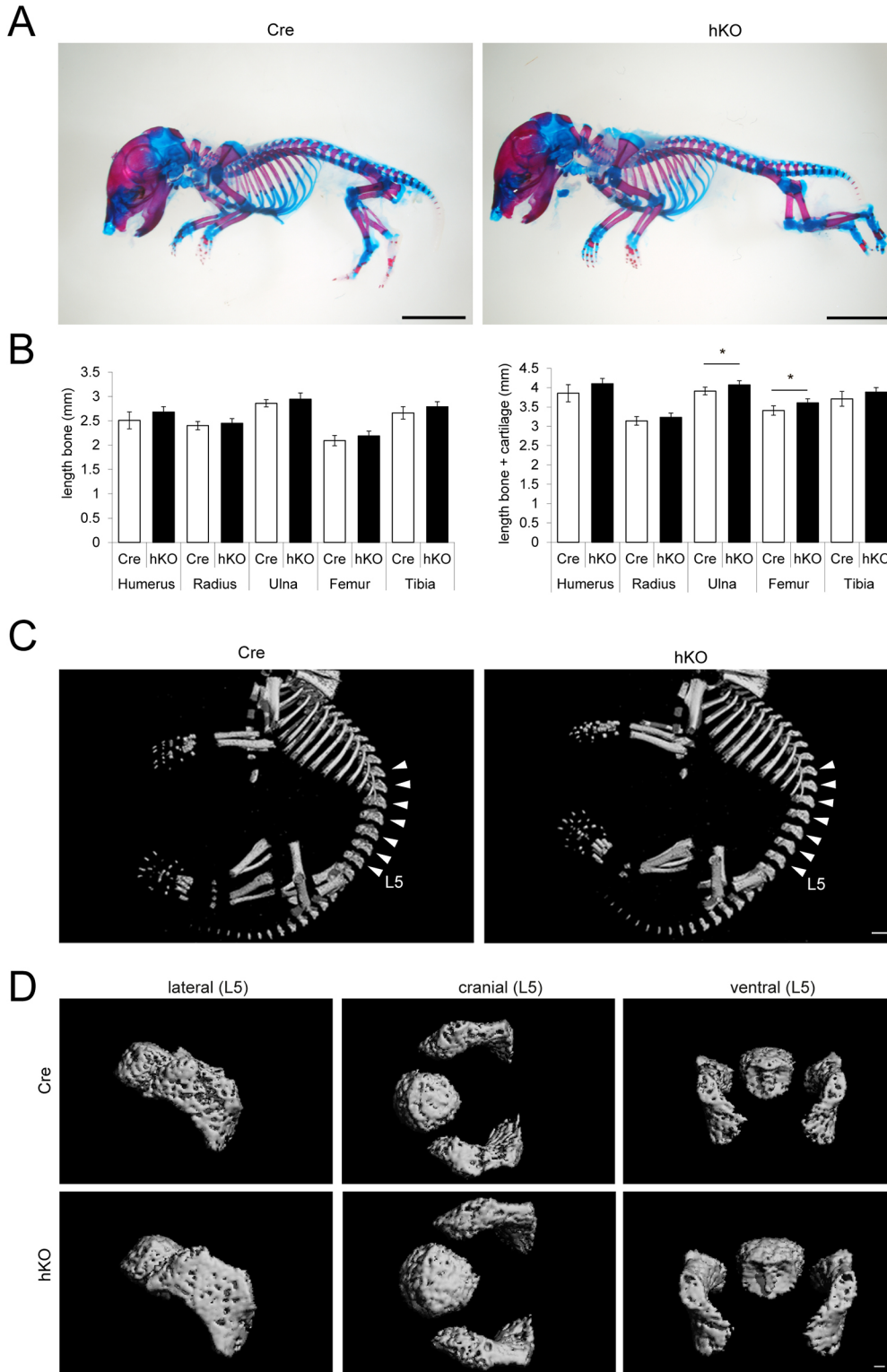


**Fig. 6. Organization of cartilaginous and bony elements in *Col2a1-Cre* and hemizygous *Col2a1-Cre-Mirc24<sup>tm1M</sup>* newborn males.** (A) Whole-mount Alcian Blue/Alizarin Red S staining of *Col2a1-Cre* (*Cre*) and *Col2a1-Cre-Mirc24<sup>tm1M</sup>* (*hKO*) males to detect cartilaginous (blue) and bony (red) structures within the skeleton. Scale bar: 5 mm. (B) The length of the bony elements (graph, left) and the length of the bony and cartilaginous parts (graph, right) were measured for humerus, radius, ulna, femur and tibia. The results of at least six mice per genotype are summarized. (C) Semi-quantitative  $\mu$ CT analysis of the skeletal system in newborn *Col2a1-Cre* (*Cre*) and *Col2a1-Cre-Mirc24<sup>tm1M</sup>* (*hKO*) males. Differences in the vertebrae between the genotypes were detected (arrowheads). Three dimensional reconstructions of the (D) femora ( $n=3$  per genotype) and the (E) 5th lumbar vertebral body are shown. The decrease of vacuous spaces in the lumbar vertebral body of *Col2a1-Cre-Mirc24<sup>tm1M</sup>* (*hKO*) males is indicated (arrows). The lateral, cranial and ventral views of the vertebral body are given. Scale bars: 1 mm in A; 100  $\mu$ m in C; 100  $\mu$ m in D.



distribution of cartilaginous (blue) and mineralized bony (red) elements in Col2a1-Cre-Mirc24<sup>tm1M</sup> males resembled that in the skeleton of Col2a1-Cre males. The rib cage architecture was normal, but the size of the skeleton appeared to be increased in Col2a1-Cre-Mirc24<sup>tm1M</sup> males. A detailed analysis of the bony and cartilaginous regions in the forelimbs and hindlimbs revealed a minor but significant increase in length for the ulna and the femur in mutant newborns compared with control (Fig. 6B). Semi-quantitative  $\mu$ CT

analysis of the newborn skeleton showed that bony elements were less porous in Col2a1-Cre-Mirc24<sup>tm1M</sup> males compared with controls (Fig. 6C, Fig. S6). The femora and vertebral bodies showed fewer vacuous interstices (Fig. 6D,E), and a greater tissue volume of the vertebral bodies of Col2a1-Cre-Mirc24<sup>tm1M</sup> males.

Bone formation is driven by endochondral ossification and we next studied bone formation and growth plate organization using safranin O and von Kossa staining (Fig. 7A). No differences in safranin O<sup>+</sup>

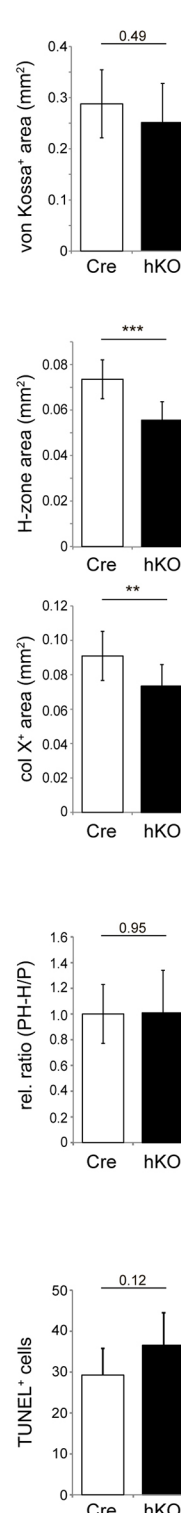
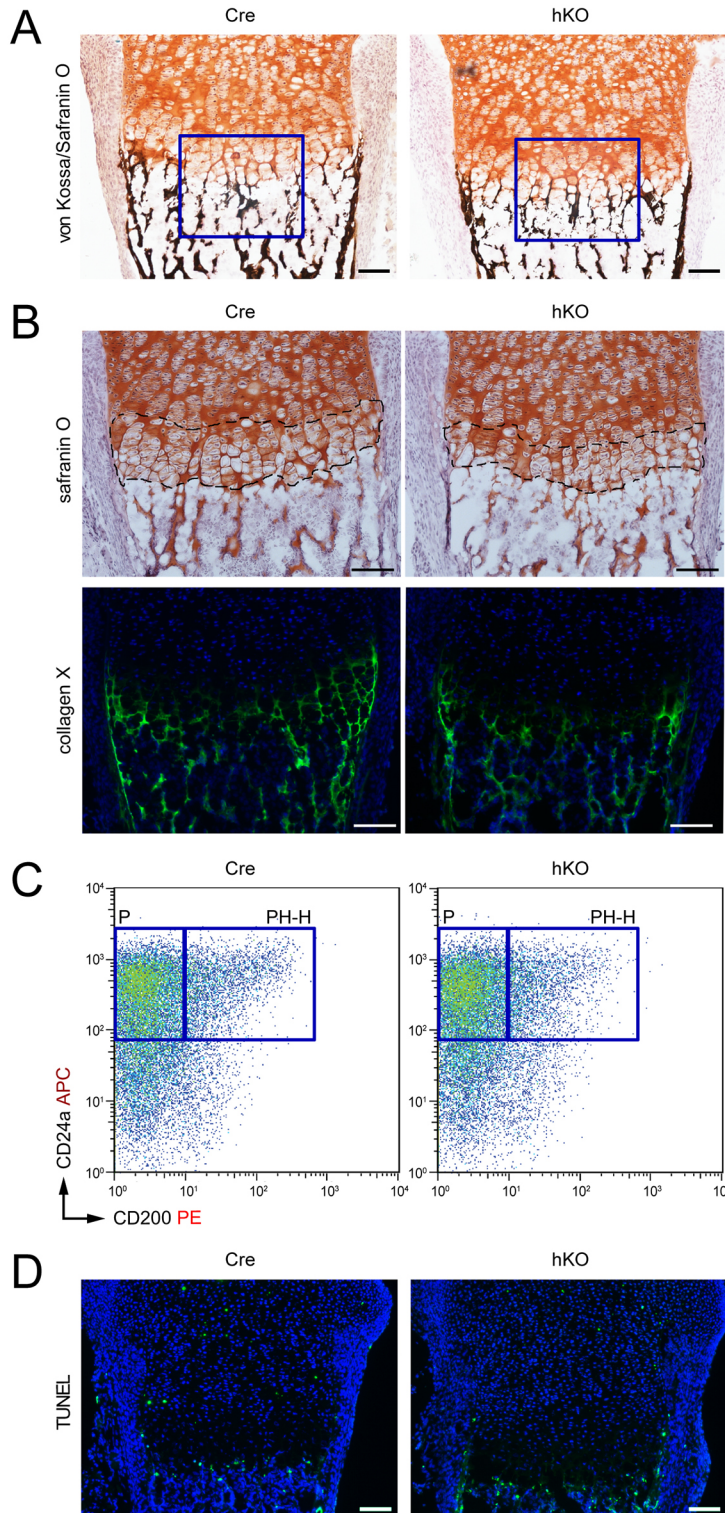


**Fig. 7. Organization of the growth plate cartilage.** Histology of in-plane matched sections from femora of Col2a1-Cre (Cre) and Col2a1-Cre-Mirc24<sup>tm1M</sup> (hKO) male newborns was assessed using (A) safranin O and von Kossa staining or (B, upper panel) safranin O staining. (B, lower panel) Collagen X protein was detected by immunostaining to define the area of hypertrophic growth plate cartilage. DAPI staining was used to detect nuclei in the growth plate. (C) Flow cytometry was applied to determine the number of CD24a<sup>+</sup>/CD200<sup>-</sup> proliferative (P) and CD24a<sup>+</sup>/CD200<sup>+</sup> prehypertrophic/hypertrophic chondrocytes in suspensions of epiphyseal cartilage from Col2a1-Cre and Col2a1-Cre-Mirc24<sup>tm1M</sup> newborns. (D) The number of dying cells in the growth plate of Col2a1-Cre and Col2a1-Cre-Mirc24<sup>tm1M</sup> newborns was characterized by TUNEL staining. DAPI staining was used to detect nuclei in the growth plate. Quantification of the von Kossa<sup>+</sup> area in the chondro-osseous junction ( $n=4$  per genotype), the hypertrophic area in histomorphological and immunological stainings ( $n\geq 7$  per genotype), the ratio of prehypertrophic/hypertrophic versus proliferative chondrocytes ( $n\geq 10$  per genotype), and the number of dying cells within the growth plate ( $n=8$  per genotype) are given. The brightness of the green signal for TUNEL staining and the blue signal for DAPI was adjusted across the images for visualization. Scale bars: 100  $\mu$ m in A,B,D.

proteoglycan (orange) distribution and in the expansion of the mineralized von Kossa<sup>+</sup> area in the chondro-osseous junction of Col2a1-Cre-*Mirc24*<sup>tm1M</sup> mice were seen, but the morphometric analysis revealed a significant decrease in the total area of hypertrophic cells (Fig. 7B, upper panel, Fig. S7). This was confirmed by immunostainings. Here, a slight decrease in the height of the collagen X-positive hypertrophic zone (Fig. 7B, lower panel) was observed, while no significant changes in the ratio of CD24a<sup>(+)</sup>/CD200<sup>(-)</sup> proliferative and CD24a<sup>(+)</sup>/CD200<sup>(+)</sup> prehypertrophic/hypertrophic (Fig. 7C) chondrocytes were detected. The number of dying chondrocytes in Col2a1-Cre-*Mirc24*<sup>tm1M</sup> mice was not significantly increased ( $P=0.11$ ,  $n=8$ ), as shown by TUNEL staining (Fig. 7D). Hence, the results of our analysis link the loss of the miR-322 to subtle changes in hypertrophic cartilage development.

### Tracheal cartilage homeostasis is impaired in mutants

However, these changes and the normal rib cage architecture cannot explain the perinatal lethality and we focused our analysis on the cartilage elements of the respiratory system. The permanent cartilage rings maintain the structure of the trachea to support the air flow and the lack of the miR-322 may affect the tracheal architecture to impair breathing in Col2a1-Cre-*Mirc24*<sup>tm1M</sup> males. Therefore, we studied the organization of isolated tracheal cartilage after staining with Alcian Blue. The trachea morphology was not significantly altered in Col2a1-Cre-*Mirc24*<sup>tm1M</sup> males, but the trachea was shortened compared with control and the diameter of the central and distal tracheal ring was significantly reduced (Fig. 8A,B). We then calculated the estimated flow rate in the trachea of Col2a1-Cre and Col2a1-Cre-*Mirc24*<sup>tm1M</sup> males. The flow rate is inversely related to the tracheal radius raised to the fourth power when considering a laminar air flow in the trachea (Bock et al., 2000); according to our calculations, the reduction of the diameter in hKO mice can cause a ~50% decrease in the calculated air flow rate in the trachea (Fig. 8C). Hence, the detected changes in the diameter have severe consequences for the air flow in the trachea. We then assessed the shape of the trachea at the 1st, 3rd and 5th tracheal ring in Col2a1-Cre and Col2a1-Cre-*Mirc24*<sup>tm1M</sup> males by histomorphological analysis. Here, we could confirm the reduction in the diameter but also detect variation in the shape in Col2a1-Cre-*Mirc24*<sup>tm1M</sup> males compared with Col2a1-Cre males (Fig. 8D). These changes are illustrated by the relative increase in the delta area difference in Col2a1-Cre-*Mirc24*<sup>tm1M</sup> males compared with the average trachea lumen of Col2a1-Cre mice (Fig. 8E,F). Air-flow reduction and variation in the shape of the trachea may heavily impair the respiratory function and lung blood circulation; we therefore analyzed the lung phenotype in newborn mice. The lung of Col2a1-Cre-*Mirc24*<sup>tm1M</sup> males was pale compared with the blood-filled lungs of Col2a1-Cre males (Fig. 8G, dotted lines, upper panel). No obvious differences in the color of the liver were observed between mutant and control (Fig. 8G, arrows, upper panel), indicating that these changes in blood circulation were restricted to the lung. Nevertheless, isolated lungs were properly developed and no differences in size or volume could be detected (Fig. 8G, lower panel). Hence, Col2a1-Cre-*Mirc24*<sup>tm1M</sup> males may die due to the insufficient air-flow rate through the trachea, insufficient oxygen supply and blood circulation in the neonatal lung. The latter is closely linked to respiratory dysfunctions (see Discussion).

### MEK1 protein levels are decreased and RAF/MEK/ERK pathway activation is stimulated in mutants

Interestingly, previous studies have demonstrated that cartilage-specific reduction of global miRNA levels (Gradus et al., 2011) or

changes in RAF/MEK/ERK pathway (Boucherat et al., 2014) also lead to skeletal abnormalities and respiratory failure, so we next studied the regulation of putative target genes in newborn femoral cartilage extracts. MEK1 levels were significantly decreased in Col2a1-Cre-*Mirc24*<sup>tm1M</sup> males, while levels of the predicted targets IGF1R, INSR, RAC1/2/3, c-RAF, PRKCl and ERK1 linked to the activation RAF/MEK/ERK remained unchanged (Fig. 9A,B). The reduction is significant, but less pronounced compared with the increase of MEK1 in miR-322 mimic-transfected PECs *in vitro*, owing to the presence of proliferative chondrocytes in total cartilage extracts (see Fig. 5B, expression in growth plate cartilage).

In addition, we analyzed the phosphorylation of ERK1/2 after insulin stimulation of isolated PECs from Col2a1-Cre-*Mirc24*<sup>tm1M</sup> and Col2a1-Cre males. Chondrocytes were stimulated with insulin and the kinetics of ERK1/2 phosphorylation were determined in immunoblots (Fig. 9C,D). Phosphorylation of ERK1/2 was induced 5, 10 and 15 min after stimulation and the signal was still detectable after 15 min in Col2a1-Cre chondrocytes. The signal was strongly increased after 5, 10 and 15 min in Col2a1-Cre-*Mirc24*<sup>tm1M</sup> chondrocytes. Total ERK1/2 levels were not affected, but MEK1 levels were decreased in Col2a1-Cre-*Mirc24*<sup>tm1M</sup> chondrocytes compared with control. The results show that, in isolated chondrocytes of Col2a1-Cre-*Mirc24*<sup>tm1M</sup> mice, RAF/MEK/ERK pathway activation is increased in the absence of miR-322 due to the decreased MEK1 levels.

Therefore, altered RAF/MEK/ERK pathway activation in Col2a1-Cre-*Mirc24*<sup>tm1M</sup> mice promotes the transformation of transient growth plate cartilage into bone, while it prevents the growth of the permanent tracheal cartilage, which results in a decrease in tracheal diameter and causes perinatal death due to respiratory failure.

### DISCUSSION

The lack of techniques to isolate sufficient RNA material from the distinct zones of the growth plate so far hindered the identification of miRNAs involved in cartilage development in mice. Here, we have used a recently developed microdissection and transcriptome profiling approach (Belluoccio et al., 2010a,b) to characterize the miRNA expression profile in the murine growth plate and describe novel miRNAs linked to cartilage differentiation.

We could show that miR-140, which was previously found to be expressed in the cartilage anlagen (Tuddenham et al., 2006), is strongly expressed throughout the different zones of the growth plate, and could demonstrate that miR-181a and miR-181a\* were increasingly expressed by prehypertrophic and hypertrophic chondrocytes. The expression of both miRNAs was originally linked to hypertrophic chondrocyte differentiation of human mesenchymal stem cells in cell culture experiments (Gabler et al., 2015) and our analysis now points to a correlation between miR-181a/miR-181a\* expression and hypertrophic chondrocyte differentiation *in situ* within the growth plate. Interestingly, miR-181a plays a key role in the differentiation and function of immune cells, modulates T-/B-cell differentiation and may act in concert with the miR-181b to regulate natural killer T-cell development via the PI3K signaling pathway (Henao-Mejia et al., 2013). Aberrant activation of this pathway is also linked to growth-plate abnormalities and skeletal overgrowth (Ford-Hutchinson et al., 2007) and the miR-181a may also target this pathway during growth plate cartilage differentiation. However, no obvious skeletal changes were reported for miR-181a/miR-181b cluster-deficient mice (Henao-Mejia et al., 2013), but here copies of similar sequence that are present on different chromosomes (miR-181a-1,

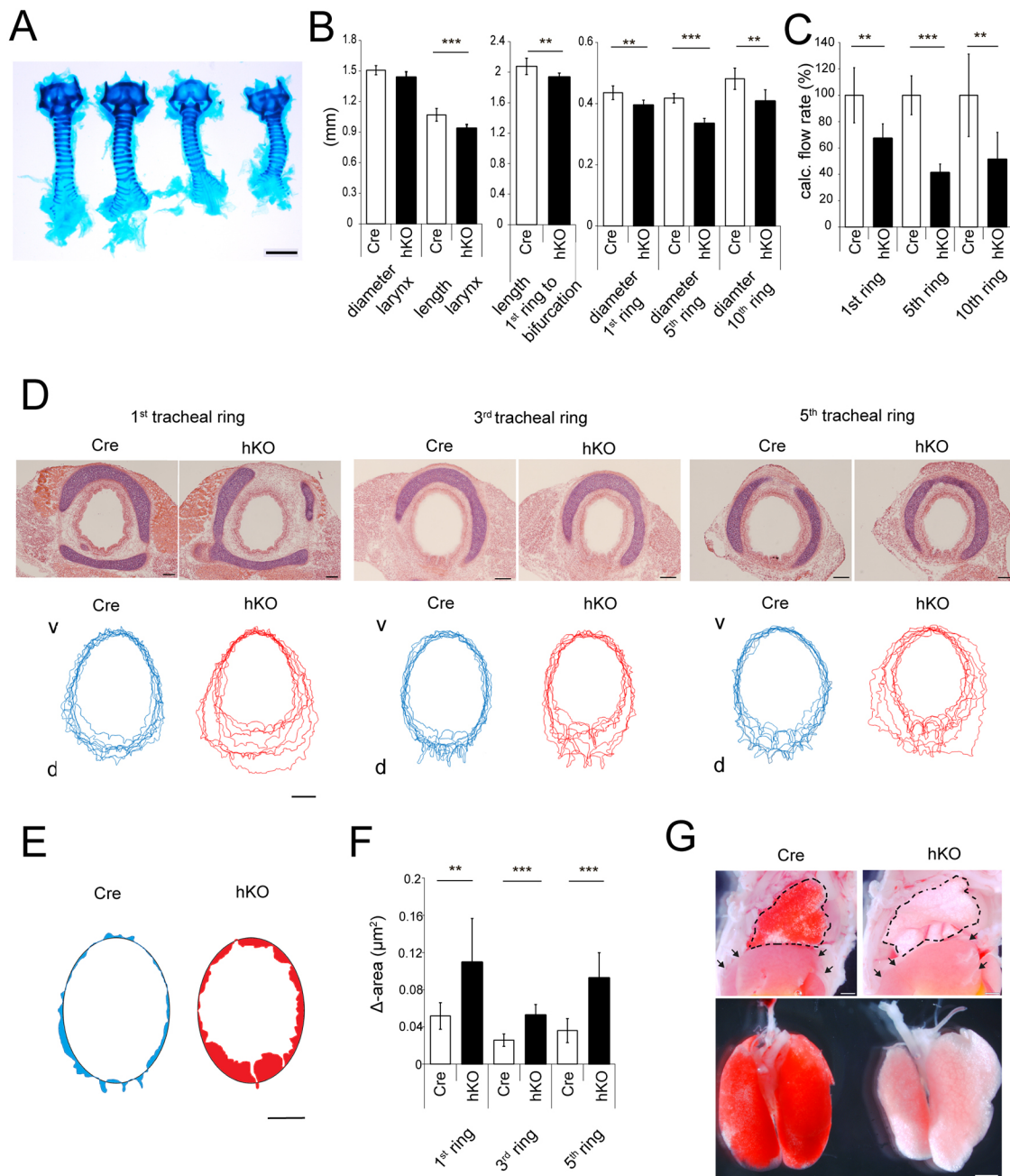


**Fig. 8. Characterization of the respiratory dysfunction.** (A) Alcian Blue staining of isolated laryngotracheal cartilage ( $n \geq 6$  per genotype). Scale bar: 1 mm. (B) The length and diameter of the cartilage elements (larynx, cartilaginous rings) were measured ( $n \geq 6$ ), and (C) the calculated flow rate for individual cartilaginous rings is given. (D) Histology of in-plane matched sections from the 1st, 3rd and 5th cartilaginous ring of Col2a1-Cre (Cre) and Col2a1-Cre-Mirc24<sup>tm1M</sup> (hKO) male newborns was assessed using Hematoxylin, Eosin and Alcian Blue staining. The shape of the tracheal lumen of individual Col2a1-Cre and hemizygous Col2a1-Cre-Mirc24<sup>tm1M</sup> newborn males is shown in overlays ( $n \geq 8$ ). v, ventral; d, dorsal. (E) Illustration of the relative area difference in the trachea lumen between a Col2a1-Cre and a hemizygous Col2a1-Cre-Mirc24<sup>tm1M</sup> newborn males in relation to the average lumen of the Cre controls. (F) The relative area differences for the 1st, 3rd and 5th cartilaginous ring were quantified. (G) Assessment of lung (dotted line) and liver (arrows) organization in the torso of Col2a1-Cre (Cre) and Col2a1-Cre-Mirc24<sup>tm1M</sup> (hKO) male mice (upper panel). Overview of dissected lungs (lower panel). Scale bars: 100  $\mu\text{m}$  in D,E; 1 mm in G.

chromosome 1, miR-181a-2, chromosome 2) may functionally compensate for the loss of a single copy in transgenic mice.

We could also identify miR-322 to be upregulated in prehypertrophic/hypertrophic chondrocytes. This miRNA was originally described to decrease IGF1R levels in the breast epithelial MCF-10A cell line (Llobet-Navas et al., 2014) and IGF1R and INSR in primary vascular smooth muscle cells to inhibit RAF/MEK/ERK pathway activation (Marchand et al., 2016). In this study MEK1 was not regulated, whereas in microvascular

endothelial cells a decrease of miR-322 levels was linked to an increase in MEK1 expression (Nakashima et al., 2010). We analyzed the expression of seven predicted targets in chondrocytes, including IGF1R and INSR, and only MEK1 was increased in miR-322 mimics-transfected (Fig. 2) or decreased in miR-322-deficient chondrocytes (Fig. 9). The luciferase assays and CRIPR/Cas-mediated genomic engineering experiments point to a direct interaction between miR-322 and *Mek1* mRNA in chondrocytes. The results illustrate that target selection of miR-322 can vary among different cell types

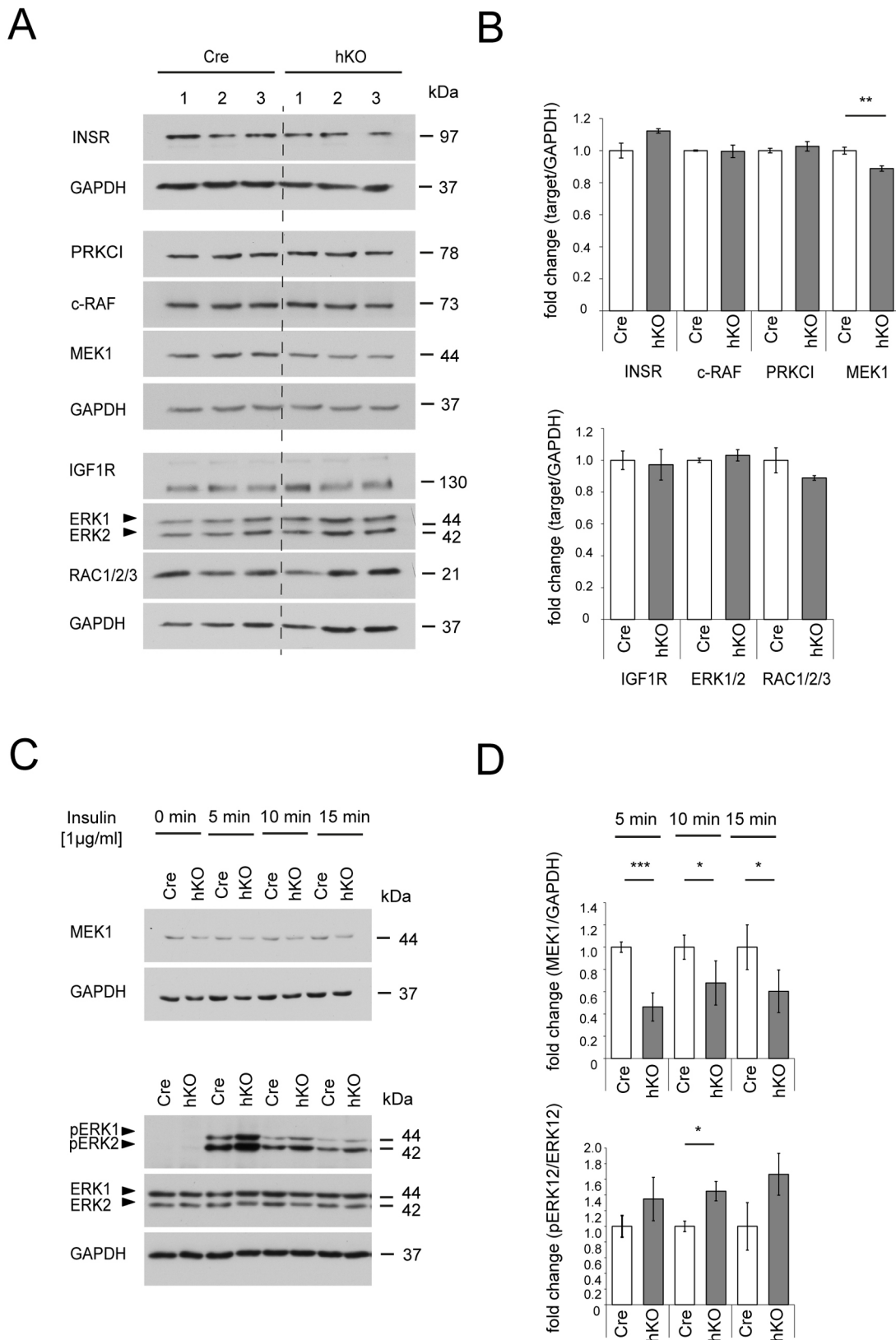


**Fig. 9. Analysis of RAF/MEK/ERK pathway activation in cartilage.** (A) Femoral cartilage extracts of Col2a1-Cre (Cre) and Col2a1-Cre-Mirc24<sup>tm1M</sup> (hKO) male newborns were analyzed for the presence of INSR, PRKCI, c-RAF, MEK1, IGF1R, ERK1/2 and RAC1/2/3 by immunoblotting. GAPDH detection was used as loading control. (B) Fold-change of targets to GAPDH ratio is shown as the analysis of three animals per genotype (graph). (C) Immunoblot analysis of MEK1 (upper panel), pERK1/2, total ERK1/2 (lower panel) and GAPDH expression after insulin stimulation in PECs isolated from Cre and hKO males. (D) The fold-changes of total MEK1 compared with GAPDH and the change in ERK1/2 phosphorylation in Cre compared with hKO PECs of three independent experiments are summarized (graphs).

and the cellular context is important to understand the molecular function of a single miRNA.

In primary chondrocytes, miR-322 stabilizes *Mek1* mRNA to increase MEK1 protein levels and inhibit the phosphorylation of the ERK1/2 pathway. The results may seem controversial, but increased kinase levels do not always activate the RAF/MEK/ERK pathway. MEK1 can form heterodimers with MEK2 to limit MEK2-mediated phosphorylation and activation of the ERK1/2 complex *in vitro* and *in vivo* (Catalanotti et al., 2009). Therefore, raised MEK1 levels in miR-322-transfected chondrocytes can prevent MEK2-mediated ERK1/2 phosphorylation, while decreased levels of MEK1 in miR-322-deficient mice can activate MEK2-dependent ERK1/2 phosphorylation to stimulate the RAF/MEK/ERK pathway.

The RAF/MEK/ERK pathway is a central target of miR-322 in chondrocytes; in cartilage this pathway is crucial for endochondral ossification and respiratory tract development. The cartilage-specific deletion of the IGF1R results in a narrow rib cage (Heilig et al., 2016), reduced tracheal cartilage diameter (J.H. and F. Zaucke, unpublished) and perinatal death due to respiratory failure (Heilig et al., 2016; Wang et al., 2011). Loss of MEK1/2 in mesenchymal tissues also manifests in a strong decrease in ERK1/2 phosphorylation, growth reduction, tracheal cartilage disorganization and neonatal death (Boucherat et al., 2014), whereas inactivation of ERK1/2 in hypertrophic chondrocytes resulted in the expansion of the hypertrophic growth plate zone and short stature of mice (Chen et al., 2015). This is in line with our results, where the increased and prolonged activation of the ERK1/2 pathway in the absence of miR-322 manifests in a slight decrease in the hypertrophic growth plate zone and a minor, but significant, length increase of skeletal elements. However, the phenotype in the absence of miR-322 was more pronounced in the tracheal cartilage than in growth plate cartilage. Here, we observed a strong reduction of the tracheal cartilage diameter with fatal consequences for postnatal respiratory tract development. These differences in the severity of the phenotype between growth plate and tracheal cartilage show that the interpretation of the ERK1/2 phosphorylation signal in chondrocytes can vary between transient and permanent cartilage.

Regulation of ERK1/2 activity by miR-322 is most important for tracheal cartilage development, as demonstrated by the perinatal lethality of Col2a1-Cre-*Mirc24<sup>tm1M</sup>* males. A previous study has already demonstrated that miRNA activity is essential for tracheal cartilage homeostasis in mice, but individual miRNAs could not be defined (Gradus et al., 2011). Our results indicate that the loss of the miR-322 signal in cartilage and its interpretation via the RAF/MEK/ERK pathway could have fatal respiratory consequences at birth. In Col2a1-Cre-*Mirc24<sup>tm1M</sup>* males, loss of the miR-322 leads to reduced tracheal diameter with a ~50% reduction of the estimated air flow and we hypothesize that this reduction prevents the transition from the fetal to the neonatal lung.

Lung blood flow is markedly reduced in the fetuses compared with newborns. At birth, fluids are removed to increase the partial pressure oxygen and supply the newborn with oxygen. This increase stimulates the release of vasoactive hormones and transforms vasoconstrictive into vasodilative blood vessels to reduce the high pulmonary resistance and strongly raise the pulmonary blood flow into the lung (Cole-Jeffrey et al., 2012; Hillman et al., 2012). Pressure and a stable trachea are required to remove the fetal fluid from the lung to initiate the 'switch' in circulation. However, in Col2a1-Cre-*Mirc24<sup>tm1M</sup>* males, the calculated flow is strongly reduced, the tracheal lumen is altered and the lung is not filled with blood. The results suggest that, in Col2a1-Cre-*Mirc24<sup>tm1M</sup>* males, respiratory function is too low to induce vasodilation and stimulate

lung blood flow. The lungs of newborns are arrested in a prenatal state and mice die due to insufficient oxygen supply.

Overall, this phenotype was surprising, as miRNA knockout mice are most often viable, fertile and with subtle phenotypes, despite the obvious effects of miRNA dysregulation in cell culture experiments (Lai, 2015; Park et al., 2012). Global deletion of the miR-322 cluster or selected miRNAs within the cluster in mice with a mixed C57BL/6N×BALB/c genetic background were originally reported to cause no evident differences within the first 2 months of life (Llobet-Navas et al., 2014). We have previously studied *Mirc24<sup>tm1M</sup>* mice with a mixed genetic background and did not observe an obvious phenotype, whereas in *Mirc24<sup>tm1M</sup>* mice with a pure C57BL/6N genetic background, perinatal lethality was observed. In *C. elegans*, the function of some miRNAs can only be determined in sensitized genetic backgrounds (Brenner et al., 2010) and, in mice, the genetic context may be as important for the outcome of a genetic inactivation of a given miRNA.

Collectively, these findings demonstrate that miR-322 is an unconventional inhibitor of the RAF/MEK/ERK pathway in chondrocytes that promotes MEK1 production and suppresses ERK1/2 phosphorylation. miR-322 may fine-tune endochondral differentiation processes and is crucial for tracheal cartilage development in mice. The human homologue miR-424 may also interact with the conserved binding site in the human *Mek1* mRNA to modulate RAF/MEK/ERK pathway-dependent chondrocyte differentiation, but its role for human growth alterations and fetal tracheal cartilage development needs to be addressed in future studies.

## MATERIALS AND METHODS

### Mice

Previously established microRNA cluster 24 (*Mirc24*) transgenic mice (*Mirc24<sup>tm1M/tm1M</sup>*), which contain a *lacZ* reporter gene to monitor expression and lox sites to inactivate the cluster-encoded miR-351, miR-322 and miR-503 (Park et al., 2012), were used. Only the latter two miRNAs are expressed in cartilage (see Fig. 1A, Fig. S5) and among those only miR-322 stabilizes *Mek1* mRNA to increase MEK1 protein levels and inhibit ERK1/2 phosphorylation (Fig. S5). Breeding protocols were used to generate floxed *Mirc24<sup>tm1M</sup>* and Col2a1-Cre mice with a C57BL/6 genetic background. Col2a1-Cre-*Mirc24<sup>tm1M/Y</sup>* males were generated by crossing floxed *Mirc24<sup>tm1M/X</sup>* female mice (Park et al., 2012) with homozygous Col2a1-Cre male mice (Ovchinnikov et al., 2000). All animal experiments were performed in accordance within the animal ethics guidelines of the German animal protection law.

### *In situ* detection of *lacZ* reporter gene activity

#### Whole-mount staining

Isolated organs and tissues were incubated in 0.2% glutaraldehyde, 5 mM EGTA, 2 mM MgCl<sub>2</sub> and 0.1 M phosphate buffer (pH 7.3) for 20 min, transferred to 50 mg/ml X-gal, 5 mM potassium ferricyanide, 5 mM potassium ferrocyanide, 2 mM MgCl<sub>2</sub>, 0.02% NP-40 and 0.1 M phosphate buffer (pH 7.3; 330 ml 0.1 M NaH<sub>2</sub>PO<sub>4</sub>, 770 ml Na<sub>2</sub>HPO<sub>4</sub>/l), and incubated for 24 h at room temperature. Samples were stored in 2 mM MgCl<sub>2</sub>, 0.02% NP-40 and 0.1 M phosphate buffer (pH 7.3) prior microscopy analysis.

### Sections

Femora were fixed overnight and stained for at least 3 h at 37°C. After embedding in OCT Tissue-Tek (Sakura Finetek), sections (at least 30 μm) were prepared using a cryostat (Leica). Sections were embedded in mounting medium (Dako) and analyzed by microscopy.

### Alcian Blue/Alizarin Red S analysis of the skeletal organization

Organs were removed from newborn mice and the carcasses were incubated for 4 days in 95% ethanol at room temperature using a rocking shaker. The samples were transferred into 0.015% Alcian Blue, 80% ethanol and 20% acetic acid staining solution and after 3 days of incubation washed for 6 h in

95% ethanol and transferred to 2% KOH. After overnight incubation at room temperature, samples were stained for 1 day in 0.03% Alizarin Red S and 1% KOH solution followed by 6 h incubation in 1% KOH. Clearance of samples was performed in 1% KOH and 20% glycerol and storage in 50% glycerol and 50% ethanol. Trachea were stained with Alcian Blue staining solution, destained with KOH and then directly stored in 50% glycerol and 50% ethanol.

### Characterization of the growth plate architecture

Cryotome sections (7  $\mu\text{m}$ ) of snap-frozen femora from newborn mice were used for histological and immunohistochemical analysis. For morphological assessment, sections were incubated in 4% paraformaldehyde (PFA) solution for 10 min at room temperature. After washing in phosphate-buffered saline (PBS), sections were stained for proteoglycans using 0.1% safranin O according to standard protocols (Romeis and Boeck, 1989) and then embedded in DPX (Sigma). The total area ( $\text{mm}^2$ ) of the hypertrophic zone and cell counts/area were determined using ImageJ software. For immunohistochemical analysis, fixed sections were predigested with 0.025% pepsin in 0.2 M HCl for 15 min at 37°C, followed by hyaluronidase digestion (5 mg/ml) for 30 min at 37°C (Sigma) and proteinase K (10  $\mu\text{g}/\text{ml}$ ) digestion for 10 min at room temperature. Sections were washed in TBS and immunohistochemical analysis was carried out with a mouse monoclonal hybridoma clone X53 identifying collagen X (1/100) (Girkontaite et al., 1996). A corresponding secondary antibody coupled to a fluorochrome (1/400, Jackson) was applied and sections were embedded in mounting medium (Dako). Bright-field as well as fluorescence images were taken (Nikon Eclipse TE2000-U Microscope). The DeadEnd Fluorometric TUNEL staining was performed according to the manufacturer's specifications (Promega). Briefly, sections were incubated in 4% PFA for 10 min at room temperature and after washing with PBS sections were predigested with proteinase K (20  $\mu\text{g}/\text{ml}$ ) for 10 min at room temperature. Sections were immersed in equilibration buffer for 10 min at room temperature and then the rTDT label reaction was performed for 1 h at 37°C. Sections were washed with 2xSSC and PBS, counterstained with DAPI and embedded. The number of TUNEL-positive cells was determined using the ImageJ software. Flow cytometry experiments with cell suspensions from growth-plate cartilage were performed with primary conjugated antibodies specific for CD24a and CD200 as previously described (Belluoccio et al., 2010a).

### Micro CT analysis

A high-resolution micro-CT scanner ( $\mu\text{CT}$  35; Scanco Medical) was used to evaluate whole-skeleton morphology and architecture in neonatal mice. Complete newborns were scanned with an isotropic voxel size of 10  $\mu\text{m}$  using, 45 kVp tube voltage, 177  $\mu\text{A}$  tube current and 400 ms integration time. Isolated femora of newborns were scanned with an isotropic voxel size of 3.5  $\mu\text{m}$  using 45 kVp tube voltage, 115  $\mu\text{A}$  tube current and 400 ms integration time. In order to remove image noise, grayscale data of the raw CT images were preprocessed using a 3D Gaussian filter algorithm and the mineralized tissue was separated from soft tissues by a global thresholding procedure (Stauber and Müller, 2008). The segmentation steps were applied with support=1.0, sigma=0.8. The image data were segmented using a threshold of 23% of the maximum grayscale value for whole skeletons, 24% of the maximum grayscale value for segmented lumbar vertebrae L5 and 32% of the maximum grayscale value for isolated femora.

### Genotype analysis

Genomic DNA was purified by standard methods and analyzed by PCR using the following sets of primers for detecting the Col2-Cre and the wild-type (488 bp) as well as the mutant (580 bp) allele of the *Mirc24* locus: Col2In1.fw, 5'-TCCAGCCCGAGCTACTTCTTAG-3'; Cre1.rw, 5'-TAATGCAGGCAAATTTGGTGTAC-3'; miR322.tmlMtm.fw, 5'-ACACACACCCTTCTGGTCTG-3'; and miR322.tmlMtm.rv, 5'-CGCTCTTCTCTGGCAT-AAG-3'.

### Cell culture

Primary chondrocytes were isolated from epiphyseal cartilage (PEC) of newborn C57BL/6N mice and cultured in DMEM (Gibco) supplemented

with 10% FCS, penicillin (100 units/ml, Biochrom), streptomycin (100  $\mu\text{g}/\text{ml}$ , Biochrom), ascorbate (44  $\mu\text{g}/\text{ml}$ , Sigma) and L-ascorbate-2-phosphate (130  $\mu\text{g}/\text{ml}$ , Sigma) at 37°C and 5% CO<sub>2</sub>. After 6 days in culture, cells were detached with collagenase 2 in DMEM (2  $\mu\text{g}/\text{ml}$  Worthington) and transfected with 50 nM mimic, 50 nM siRNA or corresponding concentrations of AllStarsNegativeControl. Cells ( $1.2 \times 10^5$ ) were resuspended in 350  $\mu\text{l}$  of medium, transferred to a 12-well plate and oligonucleotides were added in the appropriate concentration in 350  $\mu\text{l}$  OptiMEM containing the transfection solution (Qiagen). After 24 h, cells were cultured for additional 24 h in medium without FCS, in the presence or absence of 10  $\mu\text{M}$  U0126 (Pitzler et al., 2016), with or without insulin stimulation (10  $\mu\text{g}/\text{ml}$ , Sigma) and analyzed by immunoblots. Isolated chondrocytes from transgenic mice were cultured for 6 days, serum starved for 24 h, stimulated and directly used for immunoblot analysis.

The chondrogenic mouse teratocarcinoma cell line ATDC5 (Atsumi et al., 1990) (not tested for contamination) was used in high-density micromass cultures. Cells ( $3 \times 10^4$ ) were resuspended in 50  $\mu\text{l}$  medium, seeded as a drop on the bottom of a 48-well culture plate and incubated for 1 h at 37°C and 5% CO<sub>2</sub>. Medium (200  $\mu\text{l}$ ) was added and micromass cultures incubated for 14 days. Proteoglycan deposition was assessed using Alcian Blue staining and standard histology methods. In addition, RNA was isolated and used for qPCR analysis.

### Genome engineering

Two protospacer-adjacent motifs (PAMs) 89 bp upstream and 30 bp downstream of the miR-322-binding site (miR-322bs) were identified using the CRISPR Design Tool (Ran et al., 2013). The single guide sequences 20 bp upstream of the PAMs were inserted into the sgRNA-expressing plasmid pSpCas9(BB)-2A-Puro(PX459)V2.0 to generate the PX459-Mek1UTR-5'-miR-322bs and the PX459-Mek1UTR-3'-miR-322bs targeting vector. The plasmid was a gift from Feng Zhang (Broad Institute of MIT and Harvard, Cambridge, MA, USA) (Addgene plasmid 62988). For transfection  $5 \times 10^5$  ATDC5 cells were seeded in a 24-well culture plate and cultured in DMEM (Gibco) supplemented with 5% FCS at 37°C and 5% CO<sub>2</sub>. The next day, 500 ng of each targeting vector, 1.5  $\mu\text{l}$  FuGENE (Promega) and 50  $\mu\text{l}$  OptiMEM were added and incubated for 24 h. Transfection solution was replaced with selection medium containing 3  $\mu\text{g}/\text{ml}$  puromycin (Sigma) and after 4 days cells were detached with trypsin/EDTA (Biochrom). A limited dilution was performed and a single cell was seeded into an individual well of a 96-well culture plate in the presence of medium without puromycin selection. Clones were expanded and isolated DNA was screened by PCR analysis for correct deletion of the miR-322 binding site. A 560 bp fragment was amplified for the wild-type and a 445 bp fragment for the mutated sequences. Primer sequences are provided in Fig. S3. These cells were then transfected with control or mimic oligonucleotides using the transfection protocol for PEC.

### RNA isolation and quantification by microarray and quantitative PCR (qPCR)

Microdissected cartilage from 10 femora of 12-day-old mice was isolated as described (Etich et al., 2015). Total RNA from microdissected material or cultured cells was extracted with phenol-chloroform using standard methods and the RNA integrity was determined (2100 Bioanalyzer, Agilent) according to the manufacturer's specifications. The material from five epiphyseal growth plates was pooled and the Agilent protocol was applied to label and hybridize 100 ng of total RNA per single microarray of a mouse 8x15K-miRBaseV14 slide. After scanning and extraction (Agilent G2595C scanner), data were analyzed using the GenespringXII software (Agilent). Owing to the limited amount of starting material, only two independent hybridization experiments could be performed. The remaining RNA was reversely transcribed into cDNA (Qiagen) and used in miRNA miScript (Qiagen) (Etich et al., 2015) or mRNA probe-based qPCR assays (Roche, Invitrogen) (Belluoccio et al., 2010a). The expression was normalized to miR-92a or  $\beta$ -actin (*Actb*), both constantly expressed in the proliferative, prehypertrophic and hypertrophic zone of growth plate cartilage (Belluoccio et al., 2010b; Etich et al., 2015). The fold-change was calculated using the  $\Delta\Delta\text{Ct}$  method (Pfaffl, 2001).

### RNA decay assays

Mimic and AllStarsNegativeControl transfected PECs were cultured for 24 h and then 10 ng/μl actinomycin D (Enzo Life Science) was added to inhibit RNA polymerase II activity. Total RNA was isolated with phenol-chloroform extraction after 0, 4, 8, 12 and 24 h. Total RNA (5 ng) was used for quantification of relative expression levels of Mek1 by qPCR analysis. β-Actin (*Actb*) was used for normalization. The decrease in Ct values over time was determined, ΔΔCt values were calculated and the relative decrease of *Mek1* mRNA levels was used to define the turnover rate and half-life of mRNAs (Chen et al., 2008).

### Immunoblotting

Cell and cartilage lysis was performed in RIPA buffer containing 5% NP-40, 0.25% Triton X-100, 2.5% 750 mM NaCl and 100 mM Tris-HCl (pH 7.4). Lysates were homogenized using sonification (Brandson) and equal amounts of protein (20 μg) were resolved on 10% SDS-polyacrylamide gels and transferred onto nitrocellulose (Whatman). Blots were incubated for 1 h at room temperature with 5% milk powder or 5% BSA in TBS-0.1% Tween 20, and then primary antibodies against MEK1 (D2RO, 1/1000), MEK2 (13E3, 1/1000), MEK1/2 (47E6, 1/1000), ERK1/2 (1/1000), pERK1/2 (E10, 1/2000), pAKT (1/1000), AKT (11E7, 1/1000), PRKCI (C83H11, 1/2000) and RAC1/2/3 (2465, 1/2000) (all from Cell Signaling), IGF1R (1/200) and INSR (sc711, 1/200) (both from Santa Cruz), c-RAF (1/1000, V. Wixler, University Hospital Münster, Germany), and GAPDH (MAB374, 1/1500, Merck Millipore). After washing in TBS-Tween, the appropriate secondary antibodies labeled with horseradish peroxidase (DAKO) were added. Antibody binding was visualized by enhanced chemoluminescence using 10 mM Tris (pH 8.8), 12.5 μM luminol, 2.3 μM coumarin acid and 5.3 μM hydrogen peroxide solution. The chemiluminescence signal was detected using X-ray film (Valmex). Exposure was adjusted to the linear range for each of the analyzed targets. The background was subtracted using ImageJ software, samples were normalized to the control (GAPDH or non-phosphorylated kinase control) and calibrated by fixed point or the sum of replicates (Degasperi et al., 2014). A minimum of three independent experiments was performed for each immunoblot.

### Histomorphometric analysis of the tracheal lumen

Tracheae were dissected using a stereo-microscope (Nikon), embedded in OCT Tissue-Tek (Sakura Finetek) and stored at -80°C. Serial sections (10 μm) from larynx to the 5th cartilaginous ring were obtained using a cryotome (Leica) and representative section of the 1st, 3rd and 5th cartilaginous ring were stained with Hematoxylin and Eosin, and Alcian Blue as described previously (Blumbach et al., 2008). Sections were analyzed by microscopy and the shape of the tracheal lumen of Col2a1-Cre and Col2a1-Cre-*Mirc2<sup>tm1M</sup>* mice was determined. The longitudinal and transversal diameter of trachea at the 1st, 3rd and 5th cartilaginous ring of individual Col2-Cre mice were used to calculate the mean ellipsoid-like shape of the lumen (control). The relative area difference of individual tracheal lumen compared with the control was quantified using ImageJ software.

### Luciferase reporter assays

HEK293 cells (Invitrogen, not tested for contamination) were transfected with 25 nM miR-322 mimic or AllStars Negative Control and then co-transfected with 500 ng of a psiCHECK-2 vector (Promega), as previously described (Etich et al., 2015). This vector contains sequences for miRNA-specific binding sites (22 bp±5 flanking bp) or mutated binding sites of the 3'-UTR. An overview of the used oligonucleotides is given in the supplement (Fig. S2). The Dual-Luciferase Reporter Assay System (Promega) was applied to determine the luciferase activity in transfected cells.

### Statistical analysis

One-way ANOVA analysis was used to test for significance between multiple groups (Fig. 1F,G, Fig. 4B and Fig. 3E) and Bonferroni was applied for post hoc analysis. To determine statistical significance between two groups, the unpaired two-tails method of the Student's *t*-test or Mann-Whitney *U*-test (Fig. 7D, TUNEL) was used. \**P*<0.05, \*\**P*<0.01 and \*\*\**P*<0.001. Data in figures are mean±s.d.

### Acknowledgements

We thank Viktor Vixler for providing the c-RAF antibody and Feng Zhang for providing the sgRNA-expressing plasmid pSpCas9(BB)-2A-Puro(PX459)V2.0.

### Competing interests

The authors declare no competing or financial interests.

### Author contributions

Conceptualization: B. Bluhm, H.W.A.E., B. Brachvogel; Methodology: B. Bluhm, H.W.A.E., T.H., V.S.G., J.H., L.P., J.E., T.B., K.P., D.B., J.V.d.B., B. Brachvogel; Software: J.H., B. Brachvogel; Validation: B. Bluhm, H.W.A.E., T.H., V.S.G., L.P., J.E., T.B., C.F., K.P., A.N., B. Brachvogel; Formal analysis: B. Bluhm, H.W.A.E., T.H., V.S.G., J.H., J.E., T.B., A.N., D.B., J.V.d.B., B. Brachvogel; Investigation: B. Bluhm, H.W.A.E., B. Brachvogel; Resources: B. Bluhm, H.W.A.E., V.S.G., J.H., L.P., T.B., D.B., B. Brachvogel; Data curation: B. Bluhm, H.W.A.E., T.H., J.H., L.P., J.E., T.B., C.F., K.P., A.N., D.B., J.V.d.B., B. Brachvogel; Writing - original draft: B. Bluhm, B. Brachvogel; Writing - review & editing: B. Bluhm, H.W.A.E., T.H., V.S.G., L.P., J.E., T.B., C.F., A.N., D.B., J.V.d.B., B. Brachvogel; Visualization: B. Bluhm, H.W.A.E., T.H., V.S.G., J.H., J.E., T.B., B. Brachvogel; Supervision: B. Brachvogel; Project administration: B. Brachvogel; Funding acquisition: B. Brachvogel

### Funding

This work was supported by the Deutsche Forschungsgemeinschaft (DFG BR2304/5-3, BR2304/7-1, BR2304/9-1) and by Köln Fortune – Universität zu Köln (136/2013, 120/2014)

### Data availability

The arrays of the miRNA expression analysis have been deposited in GEO under accession number GSE98036.

### Supplementary information

Supplementary information available online at <http://dev.biologists.org/lookup/doi/10.1242/dev.148429.supplemental>

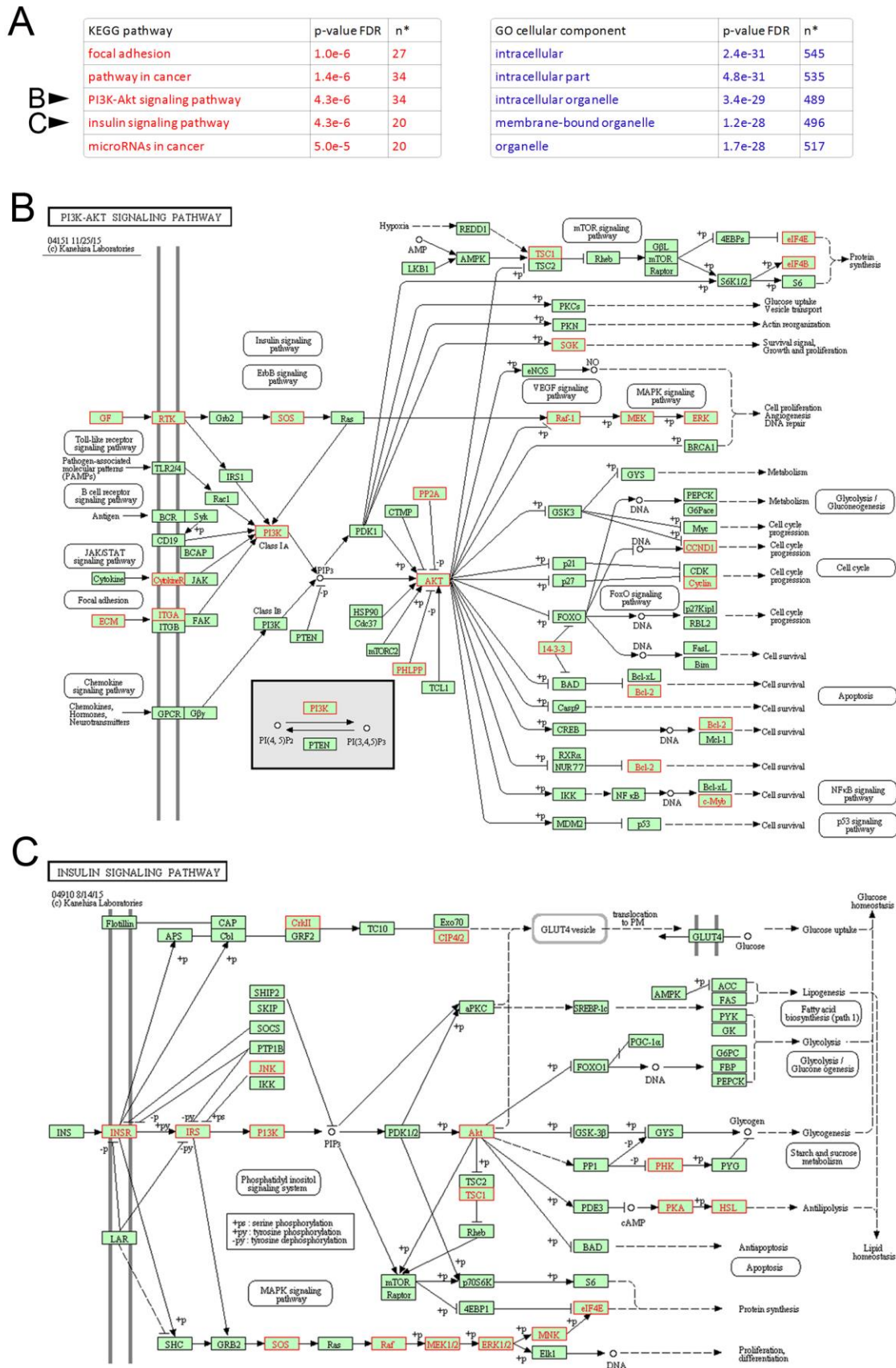
### References

- Atsumi, T., Miwa, Y., Kimata, K. and Ikawa, Y. (1990). A chondrogenic cell line derived from a differentiating culture of AT805 teratocarcinoma cells. *Cell Differ. Dev.* **30**, 109-116.
- Belluoccio, D., Etich, J., Rosenbaum, S., Frie, C., Grskovic, I., Stermann, J., Ehlen, H., Vogel, S., Zaucke, F., von der Mark, K. et al. (2010a). Sorting of growth plate chondrocytes allows the isolation and characterization of cells of a defined differentiation status. *J. Bone Miner. Res.* **25**, 1267-1281.
- Belluoccio, D., Grskovic, I., Niehoff, A., Schlötzer-Schrehardt, U., Rosenbaum, S., Etich, J., Frie, C., Pausch, F., Moss, S. E., Pöschl, E. et al. (2010b). Deficiency of annexins A5 and A6 induces complex changes in the transcriptome of growth plate cartilage but does not inhibit the induction of mineralization. *J. Bone Miner. Res.* **25**, 141-153.
- Blumbach, K., Niehoff, A., Paulsson, M. and Zaucke, F. (2008). Ablation of collagen IX and COMP disrupts epiphyseal cartilage architecture. *Matrix Biol.* **27**, 306-318.
- Bock, K. R., Silver, P., Rom, M. and Sagy, M. (2000). Reduction in tracheal lumen due to endotracheal intubation and its calculated clinical significance. *Chest* **118**, 468-472.
- Boucherat, O., Nadeau, V., Berube-Simard, F.-A., Charron, J. and Jeannotte, L. (2014). Crucial requirement of ERK/MAPK signaling in respiratory tract development. *Development* **141**, 3197-3211.
- Brenner, J. L., Jasiewicz, K. L., Fahley, A. F., Kemp, B. J. and Abbott, A. L. (2010). Loss of individual microRNAs causes mutant phenotypes in sensitized genetic backgrounds in *C. elegans*. *Curr. Biol.* **20**, 1321-1325.
- Catalanotti, F., Reyes, G., Jesenberger, V., Galabova-Kovacs, G., de Matos Simoes, R., Carugo, O. and Baccarini, M. (2009). A Mek1-Mek2 heterodimer determines the strength and duration of the Erk signal. *Nat. Struct. Mol. Biol.* **16**, 294-303.
- Chen, C. Y. A., Ezzeddine, N. and Shyu, A. B. (2008). Messenger RNA half-life measurements in mammalian cells. *Methods Enzymol.* **448**, 335-357.
- Chen, Z., Yue, S. X., Zhou, G., Greenfield, E. M. and Murakami, S. (2015). ERK1 and ERK2 regulate chondrocyte terminal differentiation during endochondral bone formation. *J. Bone Miner. Res.* **30**, 765-774.
- Cole-Jeffrey, C. T., Terada, R., Neth, M. R., Wessels, A. and Kasahara, H. (2012). Progressive anatomical closure of foramen ovale in normal neonatal mouse hearts. *Anat. Rec.* **295**, 764-768.
- Decker, R. S., Um, H.-B., Dymont, N. A., Cottingham, N., Usami, Y., Enomoto-Iwamoto, M., Kronenberg, M. S., Maye, P., Rowe, D. W., Koyama, E. et al. (2017). Cell origin, volume and arrangement are drivers of articular cartilage formation, morphogenesis and response to injury in mouse limbs. *Dev. Biol.* **426**, 56-68.

- Degasperi, A., Birtwistle, M. R., Volinsky, N., Rauch, J., Kolch, W. and Kholodenko, B. N.** (2014). Evaluating strategies to normalise biological replicates of western blot data. *PLoS ONE* **9**, e87293.
- Etich, J., Holzer, T., Pitzler, L., Bluhm, B. and Brachvogel, B.** (2015). miR-26a modulates extracellular matrix homeostasis in cartilage. *Matrix Biol.* **43**, 27-34.
- Ford-Hutchinson, A. F., Ali, Z., Lines, S. E., Hallgrímsson, B., Boyd, S. K. and Jirik, F. R.** (2007). Inactivation of Pten in osteo-chondroprogenitor cells leads to epiphyseal growth plate abnormalities and skeletal overgrowth. *J. Bone Miner. Res.* **22**, 1245-1259.
- Gabler, J., Ruetze, M., Kynast, K. L., Grossner, T., Diederichs, S. and Richter, W.** (2015). Stage-specific miRs in chondrocyte maturation: differentiation-dependent and hypertrophy-related miR clusters and the miR-181 family. *Tissue Eng. Part A* **21**, 2840-2851.
- Girkontaite, I., Frischholz, S., Lammi, P., Wagner, K., Swoboda, B., Aigner, T. and Von der Mark, K.** (1996). Immunolocalization of type X collagen in normal fetal and adult osteoarthritic cartilage with monoclonal antibodies. *Matrix Biol.* **15**, 231-238.
- Gradus, B., Alon, I. and Hornstein, E.** (2011). miRNAs control tracheal chondrocyte differentiation. *Dev. Biol.* **360**, 58-65.
- Heilig, J., Paulsson, M. and Zaucke, F.** (2016). Insulin-like growth factor 1 receptor (IGF1R) signaling regulates osterix expression and cartilage matrix mineralization during endochondral ossification. *Bone* **83**, 48-57.
- Henaoui-Mejia, J., Williams, A., Goff, L. A., Staron, M., Licon-Limón, P., Kaech, S. M., Nakayama, M., Rinn, J. L. and Flavell, R. A.** (2013). The microRNA miR-181 is a critical cellular metabolic rheostat essential for NKT cell ontogenesis and lymphocyte development and homeostasis. *Immunity* **38**, 984-997.
- Hillman, N. H., Kallapur, S. G. and Jobe, A. H.** (2012). Physiology of transition from intrauterine to extrauterine life. *Clin. Perinatol.* **39**, 769-783.
- Kobayashi, T., Lu, J., Cobb, B. S., Rodda, S. J., McMahon, A. P., Schipani, E., Merckenschlager, M. and Kronenberg, H. M.** (2008). Dicer-dependent pathways regulate chondrocyte proliferation and differentiation. *Proc. Natl. Acad. Sci. USA* **105**, 1949-1954.
- Lai, E. C.** (2015). Two decades of miRNA biology: lessons and challenges. *RNA* **21**, 675-677.
- Llobet-Navas, D., Rodríguez-Barrueco, R., Castro, V., Ugalde, A. P., Sumazin, P., Jacob-Sendler, D., Demircan, B., Castillo-Martin, M., Putcha, P., Marshall, N. et al.** (2014). The miR-424(322)/503 cluster orchestrates remodeling of the epithelium in the involuting mammary gland. *Genes Dev.* **28**, 765-782.
- Marchand, A., Atassi, F., Mougnot, N., Clergue, M., Codoni, V., Berthuin, J., Proust, C., Trégouët, D.-A., Hulot, J.-S. and Lompré, A.-M.** (2016). miR-322 regulates insulin signaling pathway and protects against metabolic syndrome-induced cardiac dysfunction in mice. *Biochim. Biophys. Acta* **1862**, 611-621.
- Matsushita, T. and Murakami, S.** (2012). The ERK MAPK pathway in bone and cartilage formation. In *Protein Kinases* (ed. G. Da Silva Xavier), Chapter 17. InTech.
- Nakashima, T., Jinnin, M., Etoh, T., Fukushima, S., Masuguchi, S., Maruo, K., Inoue, Y., Ishihara, T. and Ihn, H.** (2010). Down-regulation of mir-424 contributes to the abnormal angiogenesis via MEK1 and cyclin E1 in senile hemangioma: its implications to therapy. *PLoS ONE* **5**, e14334.
- Ovchinnikov, D. A., Deng, J. M., Ogunrinu, G. and Behringer, R. R.** (2000). Col2a1-directed expression of Cre recombinase in differentiating chondrocytes in transgenic mice. *Genesis* **26**, 145-146.
- Park, C. Y., Jeker, L. T., Carver-Moore, K., Oh, A., Liu, H. J., Cameron, R., Richards, H., Li, Z., Adler, D., Yoshinaga, Y. et al.** (2012). A resource for the conditional ablation of microRNAs in the mouse. *Cell Rep.* **1**, 385-391.
- Pfaffl, M. W.** (2001). A new mathematical model for relative quantification in real-time RT-PCR. *Nucleic Acids Res.* **29**, e45.
- Pitzler, L., Auler, M., Probst, K., Frie, C., Bergmeier, V., Holzer, T., Belluoccio, D., van den Bergen, J., Etich, J., Ehlen, H. et al.** (2016). miR-126-3p promotes matrix-dependent perivascular cell attachment, migration and intercellular interaction. *Stem Cells* **34**, 1297-1309.
- Ran, F. A., Hsu, P. D., Wright, J., Agarwala, V., Scott, D. A. and Zhang, F.** (2013). Genome engineering using the CRISPR-Cas9 system. *Nat. Protoc.* **8**, 2281-2308.
- Romeis, B. and Boeck, P.** (1989). *Mikroskopische Technik*, 17th edn. Munich, Germany: Urban & Schwarzenbeck.
- Sander, J. D. and Joung, J. K.** (2014). CRISPR-Cas systems for editing, regulating and targeting genomes. *Nat. Biotechnol.* **32**, 347-355.
- Sher, A. S. and Liu, K. J.** (2016). Congenital tracheal defects: embryonic development and animal models. *AIMS Genetics* **3**, 60-73.
- Stauber, M. and Müller, R.** (2008). Micro-computed tomography: a method for the non-destructive evaluation of the three-dimensional structure of biological specimens. *Methods Mol. Biol.* **455**, 273-292.
- Tuddenham, L., Wheeler, G., Ntounia-Fousara, S., Waters, J., Hajhosseini, M. K., Clark, I. and Dalmay, T.** (2006). The cartilage specific microRNA-140 targets histone deacetylase 4 in mouse cells. *FEBS Lett.* **580**, 4214-4217.
- Valinezhad Orang, A., Safaralizadeh, R. and Kazemzadeh-Bavili, M.** (2014). Mechanisms of miRNA-mediated gene regulation from common downregulation to mRNA-specific upregulation. *Int. J. Genomics* **2014**, 970607.
- Wang, Y., Cheng, Z., ElAlieh, H. Z., Nakamura, E., Nguyen, M.-T., Mackem, S., Clemens, T. L., Bikle, D. D. and Chang, W.** (2011). IGF-1R signaling in chondrocytes modulates growth plate development by interacting with the PTHrP/Ihh pathway. *J. Bone Miner. Res.* **26**, 1437-1446.
- Wuelling, M. and Vortkamp, A.** (2011). Chondrocyte proliferation and differentiation. *Endocr. Dev.* **21**, 1-11.



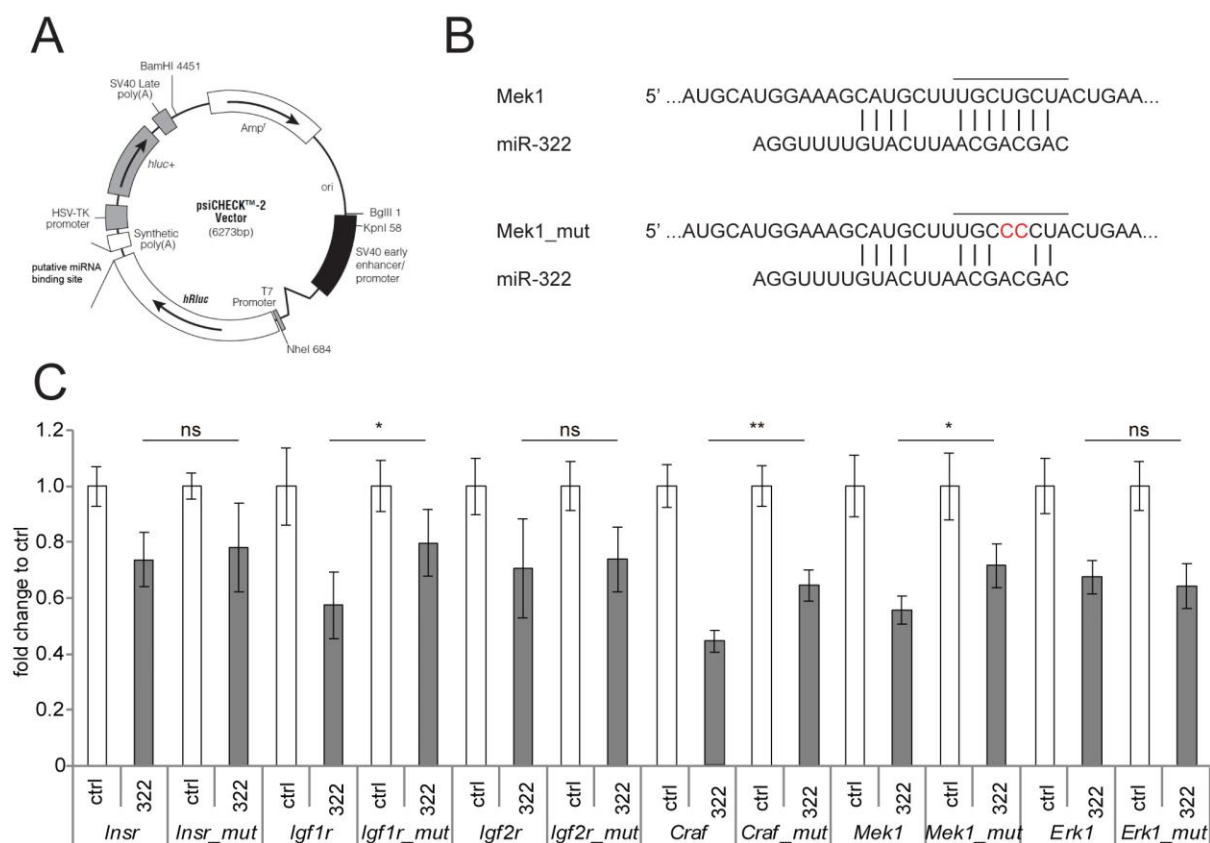
## Supplementary information



### **Supplemental figure 1**

#### **KEGG and GO cellular component analysis of miR-322 target genes expressed in growth plate cartilage**

(A) String database analysis of expressed target genes (Szklarczyk et al., 2015). The highest ranked KEGG pathway and GO cellular component terms are shown. Significance and entity numbers are given. (B) Illustration of the PI3K-AKT and (C) insulin signaling pathway according to KEGG(Kanehisa et al., 2015). Predicted targets are labeled (red).



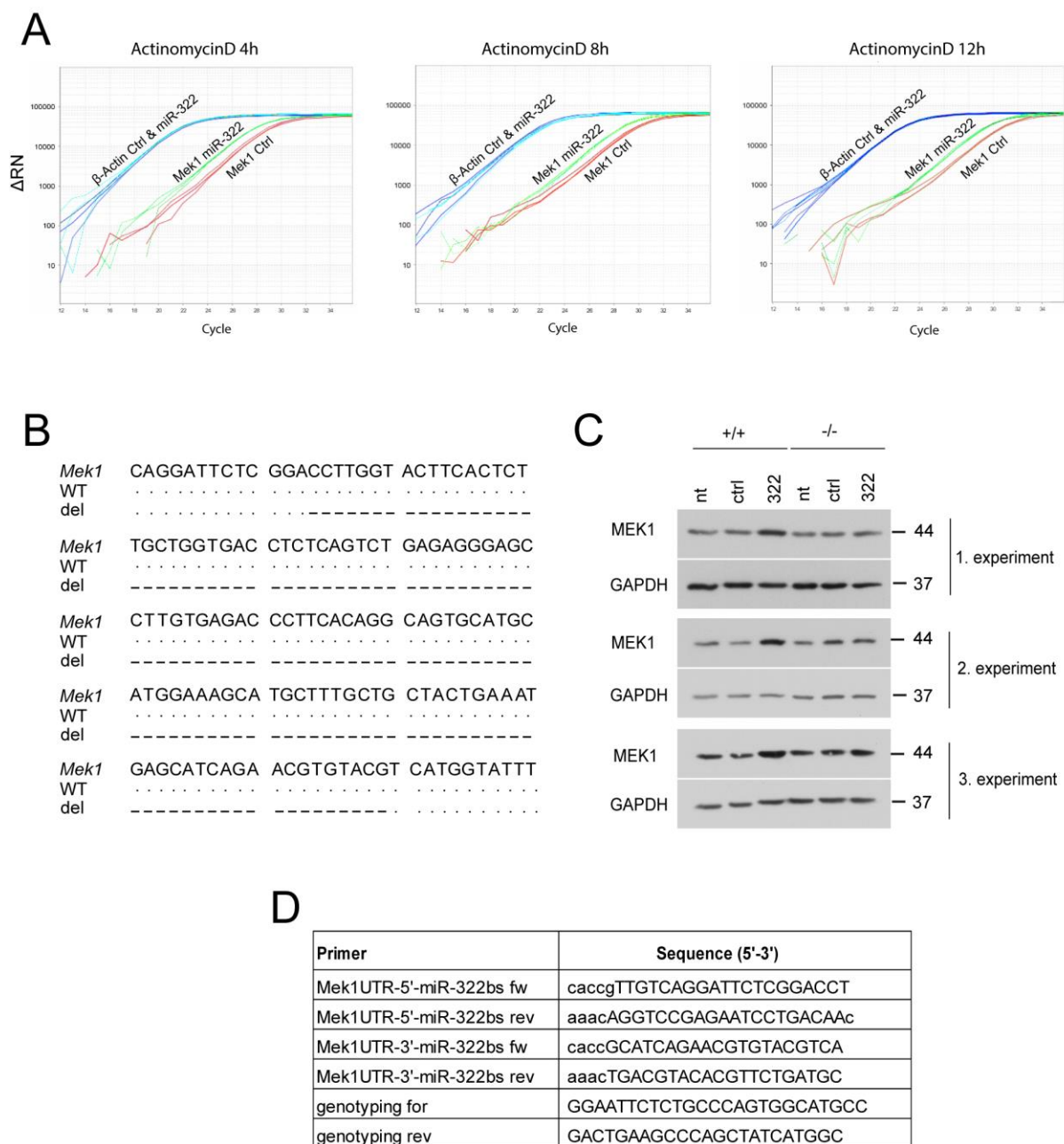
**D**

Primer	Sequence (5'-3')
Insr fw	cgcCCTCAAATTGACCAATAGCTGCTGCTTTCATAgc
Insr rev	ggccgcTATGAAAGCAGCAGCTATTGGTCAATTTGAGGgcgat
Insr_mut fw	cgcCCTCAAATTGACCAATAGCTGC <b>AA</b> CTTTCATAgc
Insr_mut rev	ggccgcTATGAAAG <b>TT</b> GCAGCTATTGGTCAATTTGAGGgcgat
Igf1r fw	cgcATCTGTACAGGAAAAGAAAAGCTGCTATTTTTgc
Igf1r rev	ggccgcAAAATAGCAGCTTTTCTTTTCTGTACAGATgcgat
Igf1r_mut fw	cgcATCTGTACAGGAAAAGAAAAGC <b>CA</b> CTATTTTTgc
Igf1r_mut rev	ggccgcAAAATAG <b>TG</b> GCTTTTCTTTTCTGTACAGATgcgat
Igf2r fw	cgcTGTGTTTGAAAAAAACCCTTGCTGCTTTAGACg
Igf2r rev	ggccgcGTCTAAAGCAGCAAGGGTTTTTTTCAAACACAgcgat
Igf2r_mut fw	cgcTGTGTTTGAAAAAAACCCT <b>TA</b> CTTTAGACg
Igf2r_mut rev	ggccgcGTCTAAAG <b>TAGT</b> AAGGGTTTTTTTCAAACACAgcgat
Craf fw	tcgagATGTTTTTGAAAAGCTGCTGCTGCTAAGGACg
Craf rev	ggccgcGTCTTAGCAGCAGCAGCTTTTCCAAAAACATc
Craf_mut fw	tcgagATGTTTTTGAAAAGCTGCTGC <b>CC</b> CTAAGGACg
Craf_mut rev	ggccgcGTCTTAG <b>GG</b> GCAGCAGCTTTTCCAAAAACATc
Mek1 fw	tcgagATGCATGGAAAGCATGCTTTGCTGCTACTGAAg
Mek1 rev	ggccgcTTCAGTAGCAGCAAAGCATGCTTTCCATGCATc
Mek1_mut fw	tcgagATGCATGGAAAGCATGCTTTGC <b>CC</b> CTACTGAAg
Mek1_mut rev	ggccgcTTCAGTAG <b>GG</b> GCAAAGCATGCTTTCCATGCATc
Erk1 fw	tcgagCTGCCACATGTAACGCCCTTGCTGCTTCTGTGg
Erk1 rev	ggccgcCACAGAAGCAGCAAGGGCGTTACATGTGGCAGc
Erk1_mut fw	tcgagCTGCCACATGTAACGCCCTTG <b>CC</b> CTTCTGTGg
Erk1_mut rev	ggccgcCACAGAAG <b>GG</b> GCAAAGGGCGTTACATGTGGCAGc

## Supplemental figure 2

### Luciferase miRNA:mRNA interaction assays

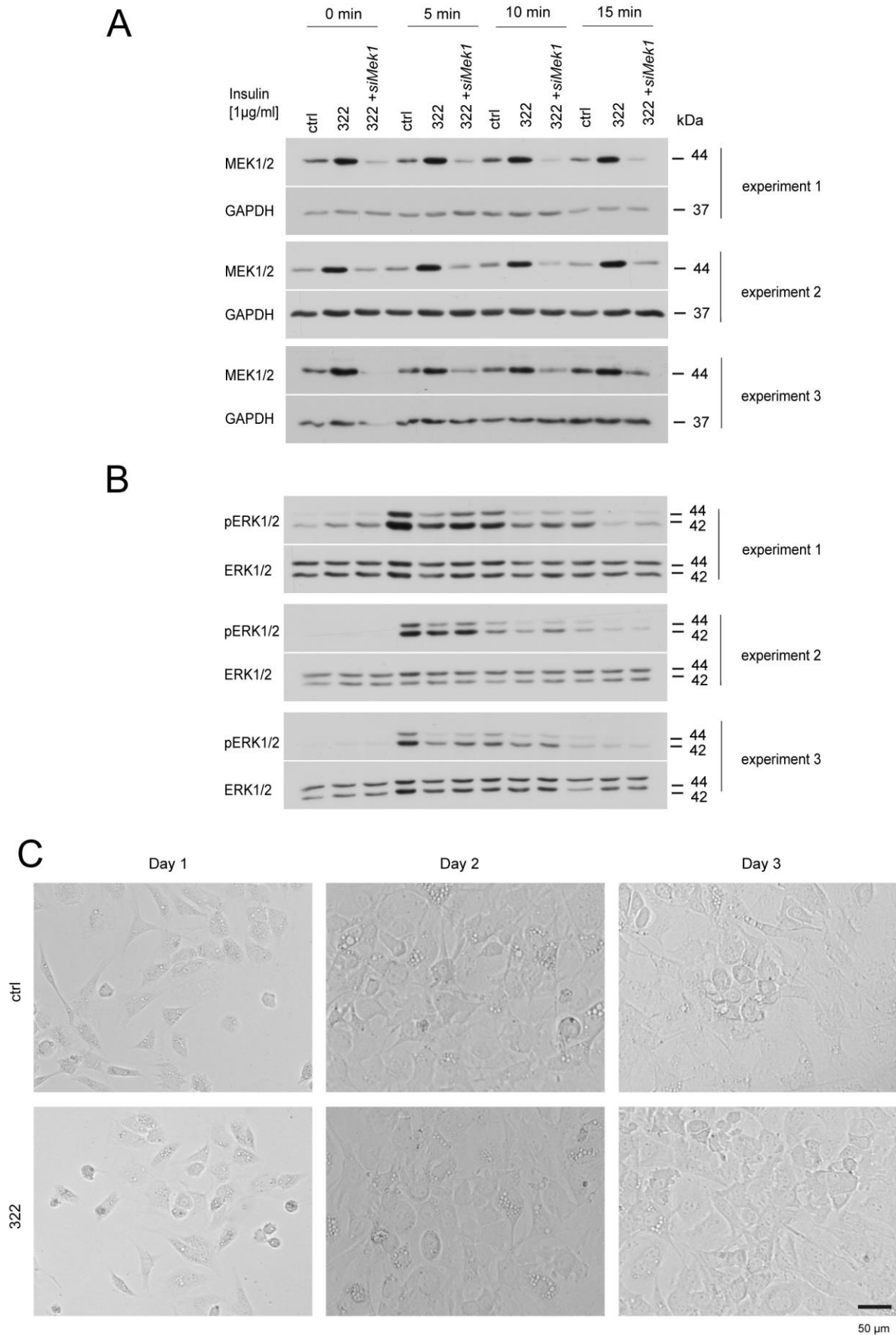
(A) Vector map of the psiCHECK2 Vector including the coding sequence of Renilla luciferase (hRluc), the multiple cloning site and the Firefly luciferase (hluc). (B) Illustration of the miR-322 and miR-322\_mut interaction with the predicted binding sequence in the 3'-UTR of Mek1. (C) Fold changes of Renilla to Firefly luciferase activity in miR-322 mimic-transfected HEK293 cells compared to control are presented ( $n \geq 3$ ) and control values with standard deviations are given (not shown in the Figure 2B due to space limitations). (D) Oligonucleotides used for the generation of luciferase reporter constructs containing the putative or mutated (red) miR-322 binding site are listed.



### Supplemental figure 3

#### qPCR analysis of mir-322 expression in actinomycin D treated mimic transfected chondrocytes

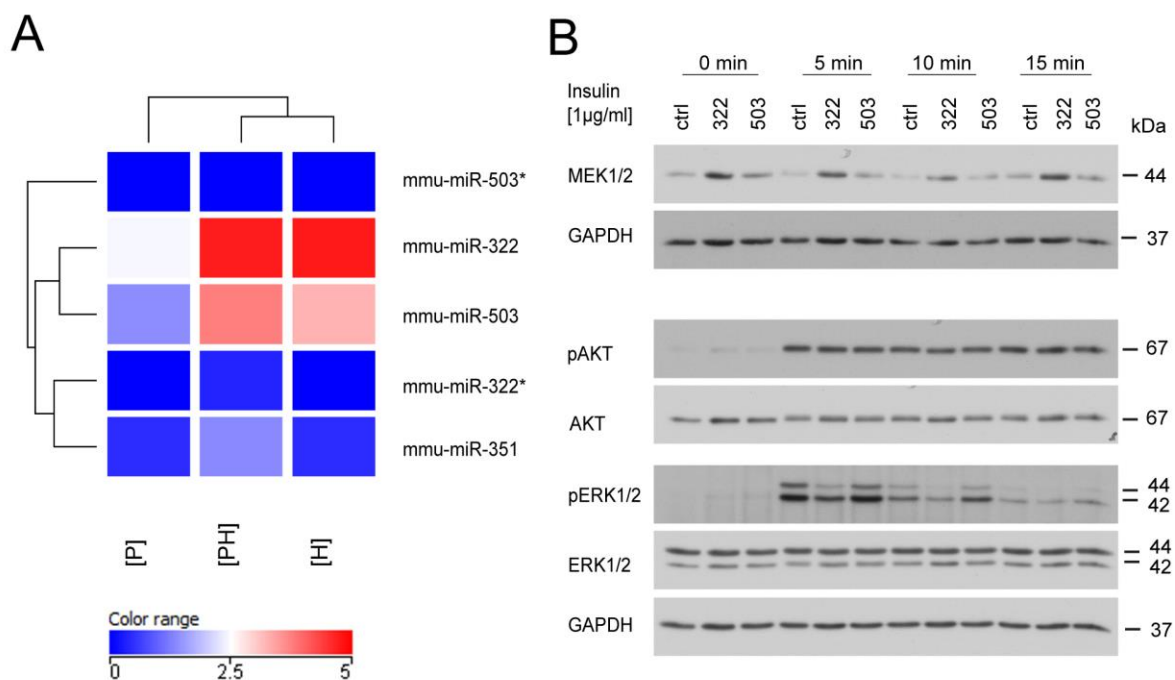
(A) Ct-plots of qPCR analysis for  $\beta$ -Actin (blue), Mek1 expression in control-(red) and miR-322 mimic-transfected (green) PECs four, eight and 12 hours after blocking transcription with actinomycin D. (B) The wild type sequence in the 3'UTR of *Mek1* is shown and the targeted sequence is marked (del, -) (C) Immunoblot analysis of total MEK1 and GAPDH levels in control and miR-322 mimic transfected ATDC5 cells containing the wild type (+/+) or biallelic deletion (-/-) of the miR-322 binding site in the 3'-UTR of *Mek1*. Three independent transfection experiments are shown. (D) Oligonucleotides used for CRISPR/Cas-mediated genomic manipulation and PCR-based genotyping are listed.



#### **Supplemental figure 4**

#### **Reduction of MEK1 protein levels and stimulation of RAF/MEK/ERK pathway activation ERK in miR-322 mimic-transfected chondrocytes using Mek1-specific siRNA**

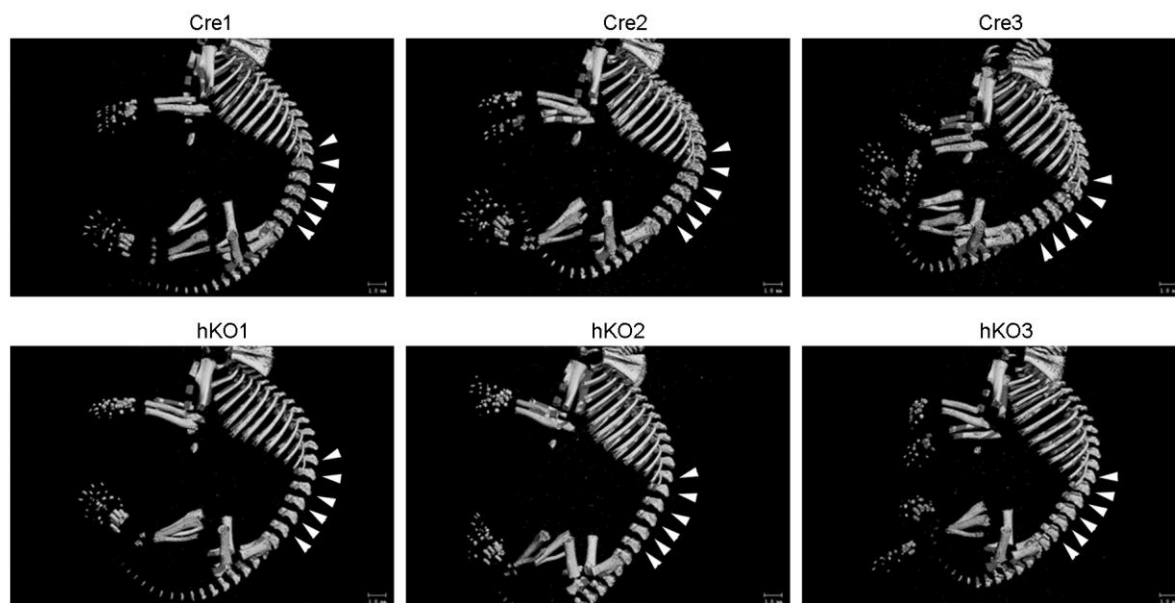
Immunoblots showing (A) total MEK1/2 and GAPDH or (B) pERK1/2 and total ERK1/2 (lower panel) in control-, miR-322 mimic- and miR-322 mimic/MEK1-siRNA-transfected PECs of three independent experiments. (C) Representative images of control- and miR-322 mimic-transfected PEC are shown for one, two and three days after transfection. No significant differences between control- and miR-322 mimic-transfected PEC were observed. Bar: (C) 50µm



**Supplemental figure 5**

(A) Intensity plots of miR-322-cluster specific miRNA expression. High (red) and low (blue) expression values are indicated. (B) Representative immunoblot analysis of pMEK1/2, total MEK1/2, pERK1/2, total ERK1/2, pAKT, total AKT and GAPDH in protein levels in control-, miR-322 mimic- or miR-503 mimic- transfected primary epiphyseal chondrocytes.

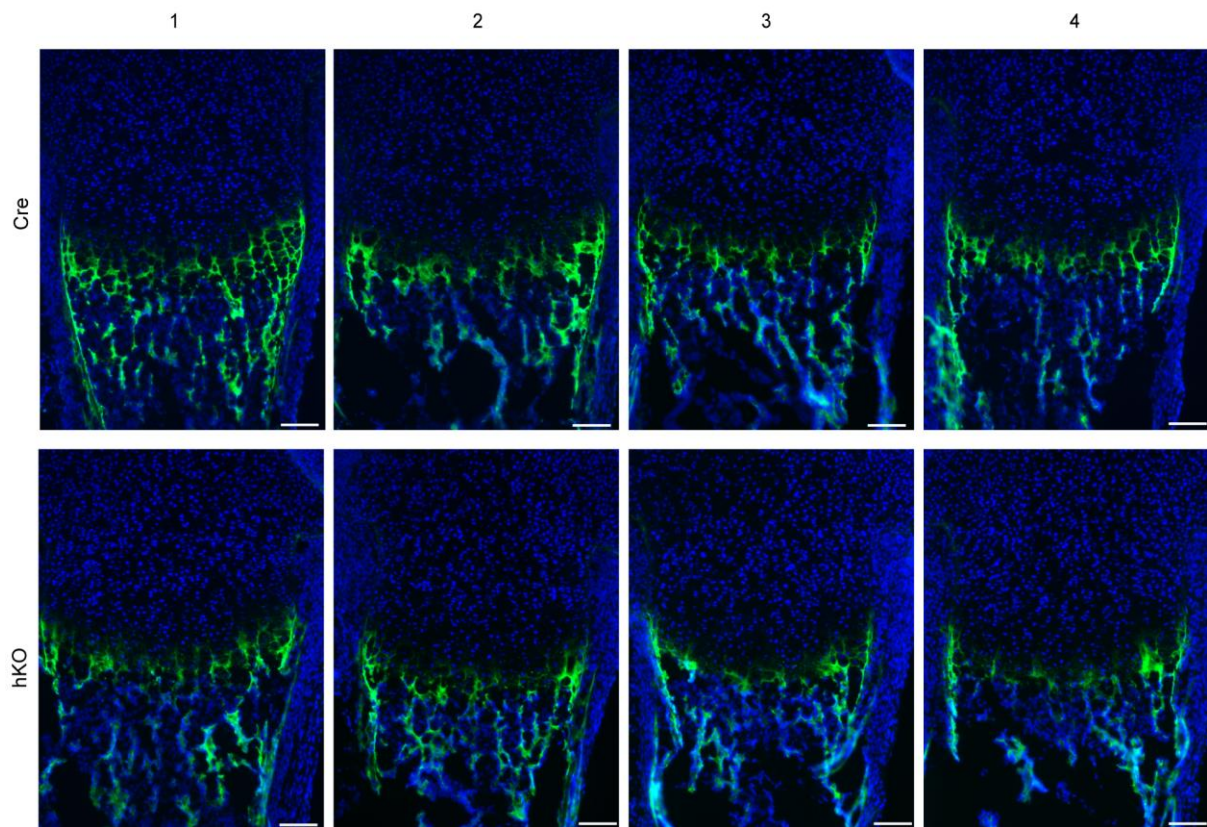




### Supplemental figure 6

#### Visualization of the skeleton in newborns

Bony elements in newborn *Col2a1-Cre* (Cre) and *Col2a1-Cre-Mirc24<sup>tm1M</sup>* (hKO) males (n=3 per genotype) were detected by  $\mu$ CT analysis. Three dimensional reconstructions are shown and the vertebral bodies are marked (arrowhead) and point to differences between the genotypes. Bars: 1mm.



### Supplemental figure 7

#### Characterization of the hypertrophic growth plate cartilage in newborns

Collagen X protein was detected by immunostaining (green) in the newborn growth plate cartilage of *Col2a1-Cre* (Cre) and *Col2a1-Cre-Mirc24<sup>tm1M</sup>* (hKO) males (n=4 per genotype). Nuclei were stained with DAPI (blue). Bar: 100 $\mu$ m